UNIVERSITÄT LEIPZIG

University of Leipzig
Faculty of Physics and Earth Sciences

Diploma Thesis

Continuous monitoring of the planetary-boundary-layer depth with lidar

in partial fulfillment of the requirements for the degree of

Diplom-Meteorologe
(Graduate Meteorologist)

submitted by
Holger Baars
on 9. Mai 2007

presented to
Prof. J. Heintzenberg and
Prof. G. Tetzlaff

Abstract

Continuous lidar observations were performed at the site of the Leibniz Institute for Tropospheric Research in Leipzig (51.35 N, 12.43 E) to determine the top height of the planetary boundary layer (PBL). The measurements were taken with the Raman lidar Polly from February 2006–January 2007. Four different methods for the determination of the PBL depth are presented. One technique, the wavelet covariance transform, was modified to permit an automated determination of PBL depth. Case studies of continuous measurements with Polly and the Doppler wind lidar WiLi are presented and discussed. Several radiosondes were launched, and temperature and humidity profiles were used to describe the thermodynamic state of the atmosphere. The achievements and the limits of the four different lidar methods for the PBL top height detection are discussed. Furthermore, the obtained PBL depths are compared to the PBL top heights derived from German Meteorological Service (DWD) Lokal-Modell (LM) data. The wavelet-covariance-transform technique with modifications was found to be the most robust method for the automated PBL depth determination procedures. A statistical analysis of the one-year data set of PBL top heights and PBL growth rates is presented and compared with respective data obtained from the LM. Mean maximum PBL depths of about 1400 m in spring, 1800 m in summer, 1200 m in fall, and 800 m in winter were found. Typical hourly and mean growth rates of 100–300 m/h were observed. It was found, that the growth of the PBL is completed between 12:00 and 15:00 local solar time in more than 80% of all analyzed cases. The comparison with the LM data reveals a general underestimation of about 20% of the PBL top height computed from LM data with respect to the Polly observations.

Zusammenfassung

Im Zeitraum von Februar 2006 bis Januar 2007 wurden am Leibniz-Institut für Troposphärenforschung (IfT) in Leipzig (51,35° N; 12,43° O) kontinuierlich Messungen mit dem Ramanlidar Polly (Portable Lidar System) durchgeführt, um die Höhe der Oberkante der planetaren Grenzschicht zu bestimmen. Es werden vier verschiedene Methoden zur Bestimmung der Grenzschichtoberkante vorgestellt. Die „wavelet covariance transform"-Methode wurde modifiziert, so dass eine automatische Bestimmung der Grenzschichtoberkante mit Lidar möglich ist. Anhand verschiedener Fallstudien werden Messungen von Polly und dem Doppler-Wind-Lidar WiLi ausführlich diskutiert. Temperatur- und Feuchteprofile von Radiosondenaufstiegen werden genutzt, um den thermodynamischen Zustand der Atmosphäre zu beschreiben. Dabei werden die Möglichkeiten und Grenzen der vorgestellten Methoden zur Bestimmung der Grenzschichtoberkante diskutiert. Hierbei wurde herausgefunden, dass die modifizierte „wavelet covariance transform"-Methode am geeignetsten für die automatische Datenauswertung ist. Desweiteren wurden die vom Lokal-Modell (LM) des Deutschen Wetterdienstes (DWD) berechneten Höhen der Grenzschichtoberkante mit den experimentell bestimmten verglichen. Eine Statistik der Grenzschichtdicken und deren Anstiegsraten aus dem vorliegenden einjährigem Datensatz wird präsentiert, genauso wie ein Vergleich mit den vom LM erhaltenen Grenzschichtdicken. Mittlere maximale Höhen der Grenzschichtoberkante von 1400 m im Frühling, 1800 m im Sommer, 1200 m im Herbst und 800 m im Winter wurden beobachtet. Typische stündliche und mittlere Anstiege der Grenzschichtdicke liegen zwischen 100 und 300 m/h. In mehr als 80% der analysierten Fälle war das Wachstum der Grenzschicht zwischen 12:00 und 15:00 Uhr lokaler Sonnenzeit abgeschlossen. Der Vergleich mit dem LM zeigt eine deutliche Unterschätzung der Höhe der Grenzschichtoberkante im Bezug auf die Polly-Messungen von ca. 20%.

Contents

Chapter 1

Introduction

The planetary boundary layer (PBL) is that part of the troposphere that is directly influenced by the presence of the earth's surface, and responds to surface forcings with a timescale of an hour or less (Stull 1988). These forcings include frictional drag, evaporation and transpiration, heat transfer, and pollution emissions. The PBL depth is variable in time and space, ranging from hundreds of meters to a few kilometers. It is one key parameter in the description of vertical processes in the lower troposphere. The diurnal cycle of the PBL top height strongly determines the environmental state at the surface over the day. Therefore, it is an important input parameter for air-quality models. Observations of the PBL depth with high vertical and temporal resolution are thus desirable. The top height of the PBL can be determined from vertical profiles of temperature, humidity, wind, and pollutants, such as aerosol particles. These profiles can be derived from, e.g., radiosonde, radio acoustic sounding system (RASS), wind profiler (Angevine et al. 1998), ceilometer (Eresmaa et al. 2005), lidar (Lammert and Bösenberg 2005), and sodar (Russel and Uthe 1978). All of these instruments have restrictions concerning weather conditions, spatial and temporal resolution, and accuracy.

Lidar appears to be a promising tool for an accurate, automated detection of the PBL top height with high resolution in time and space. Because the PBL usually contains more aerosol particles than the free troposphere, and thus has a higher backscatter intensity, lidar-derived backscatter profiles can be used to determine the PBL depth. Since August 2005 a small, compact Raman lidar (Polly: Portable lidar system) is run almost continuously at the Leibniz Institute for Tropospheric Research (IfT) in Leipzig (51.35 N, 12.43 E, central Europe). Routine daily measurements from 00:01–02:14 UTC and 12:01–14:14 UTC are performed. Since January 2006 five-minute observations with 30 s resolution are made once per hour to measure the diurnal PBL

development. An automated algorithm was developed to visualize the data (see website: http://iftwetter.tropos.de:8083/VAP/).
Field studies with automated data processing have been presented for various, almost ideal convective conditions by applying the gradient method (Menut et al. 1999), the variance method (Hooper and Eloranta 1985), the wavelet-covariance-transform method (Cohn and Angevine 2000) and the fitting method (Steyn et al. 1999). However, the detection of the PBL top can be challenging when conditions in the PBL depart from the ideal of a well-mixed, cloud-free PBL (Brooks 2003). It is essential for long-term measurements to analyze data automatically and to assure a high level of accuracy for various meteorological conditions. This issue is the main topic of this work. An automated algorithm for the determination of the PBL top height from measurements with Polly was developed. The preferred wavelet-covariance-transform (WCT) method was intensively compared with other potential methods (gradient, variance, and fitting methods). The results were also compared to PBL top heights as derived from the Lokal-Modell (LM) of the German Meteorological Service (DWD). Finally, the automatically retrieved PBL depths from a one-year data set are statistically analyzed.
In Chapter 2, a short theoretical background regarding the evolution of the PBL is given. The turbulence-kinetic-energy budget equation, the diurnal cycle of the PBL, and basic methods for the determination of the PBL depth are discussed. In Chapter 3, the automated lidar measurements are described. The lidar equation and the Polly setup are presented. Chapter 4 deals with the description of the lidar data processing. First, the WCT method after Brooks (2003) is explained, followed by modifications made to allow an automated data analysis and PBL top height detection. Furthermore, other available techniques for the PBL top height detection with lidar are discussed. Chapter 5 presents the PBL depth determination from LM data as done by the DWD. It follows a short description of auxiliary information obtained with the wind lidar WiLi and with radiosonde. In Chapter 6, results of the different methods for the determination of the PBL depth are discussed and compared to the LM-derived PBL top heights for several case studies. Radiosonde profiles and wind-lidar data (vertical wind) are used to characterize the convective state of the PBL. The diurnal cycle of the PBL is studied as well. Chapter 7 presents the statistical analysis of a one-year dataset of PBL top heights measured from February 2006 to January 2007. PBL depths and daily PBL growth rates are discussed and, again, compared with respective data provided from the LM. A summary is given in Chapter 8.

Chapter 2

Planetary boundary layer

This chapter presents the definition of the PBL top height and the processes that control its diurnal evolution. The budget equation of turbulence kinetic energy is discussed. Furthermore, methods for the determination of the PBL top height are explained.

2.1 Vertical structure of the troposphere

The troposphere can be divided into the PBL close to the surface, characterized by turbulence, and the free troposphere, where the large-scale atmospheric flow controls the local wind field. Because the generated turbulence causes mixing within the PBL, substances and atmospheric quantities with sources at the surface disperse horizontally and vertically within this layer in the absence of significant sinks. Vertical profiles of aerosol concentration, trace gases such as water vapor, and temperature can be used to derive the depth of the PBL. An example is given in Fig. 2.1. A vertical profile of virtual potential temperature Θ_v and water-vapor-to-dry-air mixing ratio s derived from a radiosonde launch at the IfT site in July 2006 is shown. Two different layers of air can be identified. Almost constant values of virtual potential temperature Θ_v and high values of s can be seen within the PBL, whereas the free troposphere is characterized by low moisture and stable stratification. The top of the PBL, z_i, is defined as the altitude where air from the PBL and the free troposphere is found in equal proportion (Menut et al. 1999). The vertical extent of the region where both air characteristics can be observed is called transition zone (Brooks 2003). In Fig. 2.1 the transition zone exceeds from 1750 to 2250 m, so that z_i=2000 m.

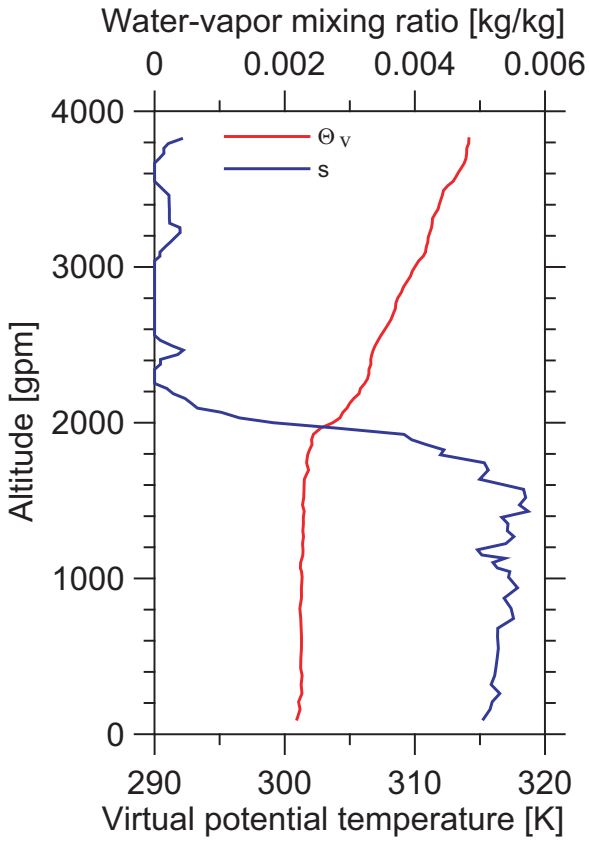

Figure 2.1: Radiosonde profiles of virtual potential temperature Θ_v and water-vapor-to-dry-air mixing ratio s observed at Leipzig (IfT) on 4 July 2006, 12:40 UTC.

2.2 Turbulence kinetic energy

The vertical transport of quantities within the PBL is caused by turbulence. The turbulence kinetic energy (TKE) can be used as a measure of the intensity of turbulence. The average TKE per unit mass is defined as

$$\overline{e} = \frac{1}{2}\overline{u_i'^2}, \tag{2.1}$$

with

$$u_i' = u_i - \overline{u_i}. \tag{2.2}$$

u_i', with $i = 1, 2, 3$, are the three turbulent wind components calculated from the difference of the observed wind u_i and the mean wind $\overline{u_i}$.
It is possible to define terms that describe production and loss mechanisms for TKE

in the PBL by analyzing the budget equation of $\overline{e}$:

$$\underbrace{\frac{\partial \overline{e}}{\partial t}}_{I} + \underbrace{\overline{u}_j \frac{\partial \overline{e}}{\partial x_j}}_{II} = \underbrace{\delta_{i3} \frac{g}{\Theta_v} \left(\overline{u_i' \Theta_v'}\right)}_{III} \underbrace{- \overline{u_i' u_j'} \frac{\partial \overline{u_i}}{\partial x_j}}_{IV} \underbrace{- \frac{\partial \left(\overline{u_j' e}\right)}{\partial x_j}}_{V} \underbrace{- \frac{1}{\overline{\rho}} \frac{\partial \left(\overline{u_i' p'}\right)}{\partial x_i}}_{VI} \underbrace{- \epsilon}_{VII}. \tag{2.3}$$

Einstein's summation notation is used here. $x_{i,j}$ are the Cartesian coordinates of the corresponding wind components and t is the time. Θ_v' and p' are the turbulent components of virtual potential temperature Θ_v and pressure p, respectively. g describes the acceleration due to gravity and $\overline{\rho}$ is the mean density of air. ϵ is the TKE dissipation rate. In the following, the vertical coordinate x_3 is denoted as z and the corresponding wind component u_3 as w.

Terms I and II in Eq. (2.3) describe the temporal change and the advection of TKE at a given site, respectively. The buoyancy term (III) expresses the thermal generation or loss of turbulence. The most important part in this term is the vertical turbulent flux of virtual potential temperature $\overline{w'\theta_v'}$. According to the K-theory, turbulent fluxes can be parameterized with the local mean gradient of the transported quantity and a positive eddy-transfer coefficient K (Stull 1988). This leads to

$$\overline{w' \Theta_v'} = -K \frac{\partial \overline{\Theta_v}}{\partial z}. \tag{2.4}$$

K is not constant and differs depending on the quantity transported. It varies with the size of the eddies, and an increase with height is typically observed. This parameterization is a small-eddy closure technique and frequently fails for larger eddies, but it is still used for many applications.

As can be seen from Eq. (2.4), $\overline{w' \Theta_v'}$ depends on the static stratification and can thus be positive or negative for unstable or stable situations, respectively. In the absence of advection of cooler or warmer air, it is controlled by the incoming radiation, and thus typically positive during day and negative during nighttime. Under unstable conditions, the buoyancy production rate of TKE (Term III) has positive values well above the surface up to approximately the top of the PBL. When clouds form, a positive value can be observed throughout the entire cloud layer, except for heights around the cloud base where static stability prevails. Turbulence caused by buoyancy is also called thermal turbulence.

Term IV represents the mechanical turbulence production and is usually positive. Using the K-theory this term can be written as

$$- \overline{u_i' u_j'} \frac{\partial \overline{u_i}}{\partial x_j} = K \frac{\partial \overline{u_i}}{\partial x_j} \frac{\partial \overline{u_i}}{\partial x_j} = K \left(\frac{\partial \overline{u_i}}{\partial x_j} \right)^2. \tag{2.5}$$

Since the wind shear, $\frac{\partial \overline{u_i}}{\partial x_j}$, is strongest at the surface, the maximum shear production of $\overline{e}$ is observed close to the ground. It rapidly decreases with height. A smaller shear production rate can be observed at the top of the PBL and near the nocturnal low-level jet. Shear production is controlled by the wind speed and typically the only process which produces TKE at nighttime.
Turbulent transport of $\overline{e}$ is described by Term V. Significant transport of TKE is mainly observed in vertical direction within the PBL. For convective cases, this results in a net transport of TKE from the lower part to the upper part of the PBL (Garratt 1992). Integrated over the entire PBL, Term V is close to zero.
The pressure correlation term (VI) describes the contribution of waves, e.g., internal gravity waves to TKE. Dissipation of TKE is considered in Term VII. Dissipation rates decrease rapidly with height and are dependent on the magnitude of $\overline{e}$.
In summary, the buoyancy term and the shear term are TKE production terms. Terms V and VI are often combined to one transport term, because they describe the distribution of TKE within the PBL. The dissipation term (VII) leads always to a loss of $\overline{e}$. Thus, the depth of the PBL strongly depends on the strength of the production terms (III and IV).
Fig. 2.2 shows the buoyancy production versus the shear production. When the buoyancy production is more than a factor of three larger than the shear production, the regime is called "free convection". In the forced-convection regime, wind shear is the dominant force of turbulence production. The shear term (IV) is then more than a factor of three larger than the absolute value of the buoyancy term (III). No turbulence is observed when the buoyancy term (III) is negative and the shear production term (IV) is less than its absolute value.
Shear production rates decrease more rapidly with height than buoyancy production rates (Oke 1987). Therefore, PBL dominated by free convection are usually deeper than the ones in which forced convection prevails.

2.3 Diurnal cycle of the PBL

The diurnal cycle of the PBL is illustrated in Figure 2.3. After sunrise, when the solar radiation is strong enough to supply sufficient heat, the nocturnal inversion at the ground breaks up. Now, a statically unstable situation is observed in the lower air layers. Rising and sinking thermals mix atmospheric properties and substances up to a height above which the atmosphere becomes stably stratified. The layer where mixing due to free convection takes place is called the "convective mixed layer". The

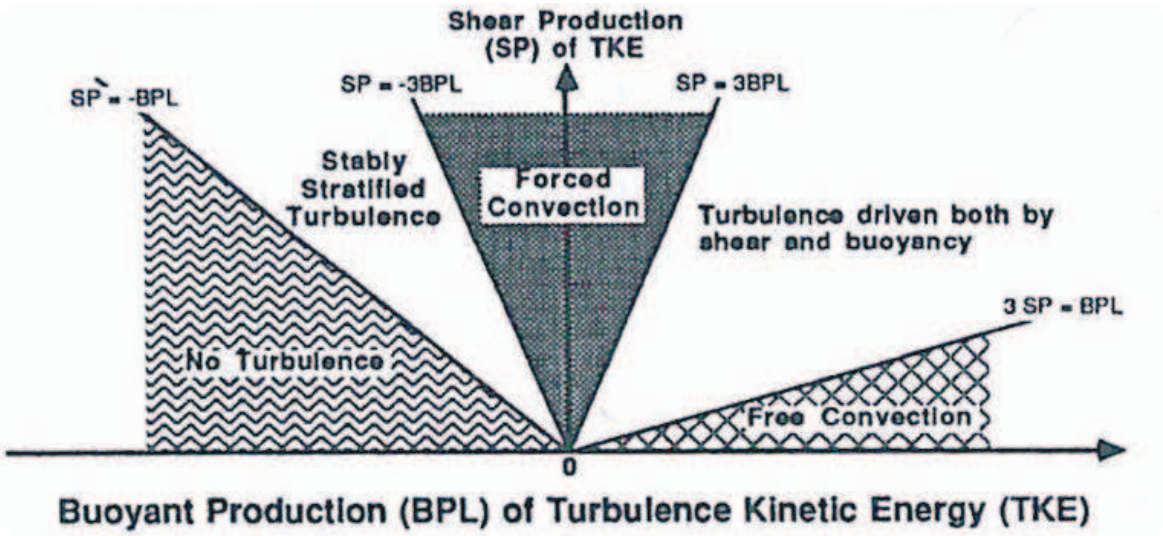

Figure 2.2: Regimes of turbulence (Stull 1988). BPL is related to Term III and SP to Term IV in Eq. (2.3).

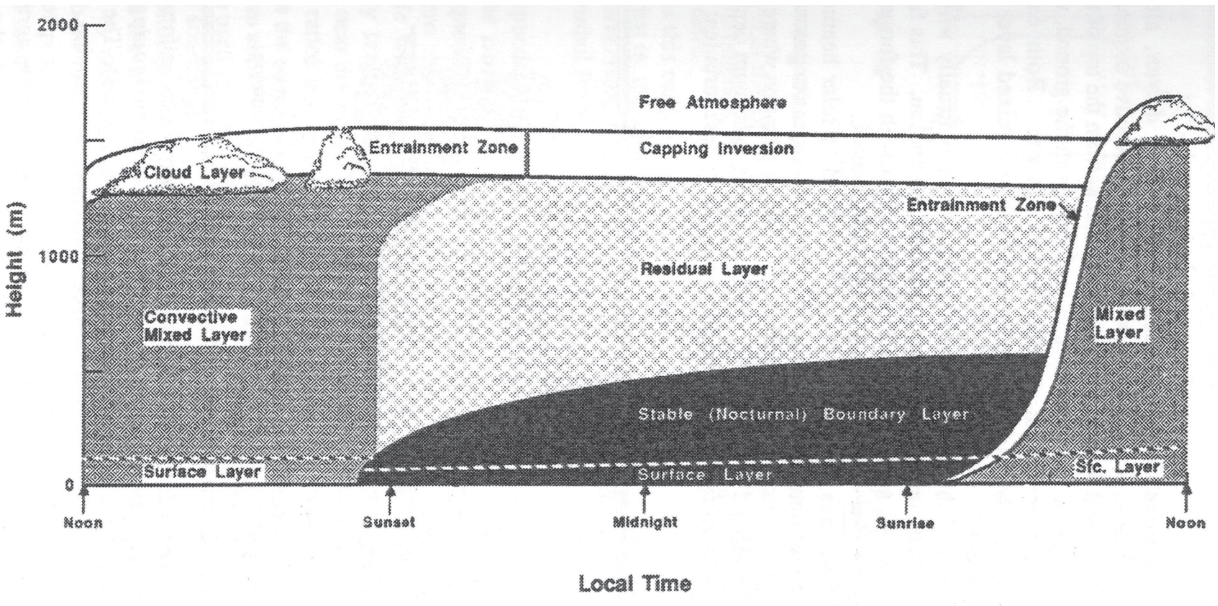

Figure 2.3: Typical boundary-layer evolution (Stull 1988).

statically stable layer above the convective mixed layer is the transition zone, often also denoted as entrainment zone, which is followed by the free troposphere. According to the definition in Sec. 2.1, the PBL reaches up to the middle of the transition zone. If free convection takes place, the PBL is called a convective PBL in the following.
Due to entrainment of free-tropospheric air into the PBL, its depth grows. When the relative humidity exceeds the saturation level in the rising bubbles, clouds form. By the release of latent heat the clouds can easily penetrate into the free troposphere. In case of cloud formation, the PBL is divided into a cloud and subcloud layer.
A few hours before sunset convection becomes weaker and finally vanishes completely. The mixing process stops. During nighttime, a new statically stable PBL forms, caused by the cooling of the near-surface air. Now, the lower troposphere consists of the PBL and the residual layer (RL), i.e. the residual part of the former daytime PBL. Turbulence in this stable or nocturnal PBL is typically mechanically driven and can be very weak. If a wind shear is existing, e.g., due to a nocturnal jet, it causes mixing throughout the PBL and also within the lowest part of the RL, which leads to a growth of the depth of the nocturnal boundary layer. As stated above, forced convection is limited to a region close to the surface. Thus, the depth of the nocturnal boundary layer is typically less than 500 m (Stull 1988).

2.4 Determination of the PBL top height

In the following, three basic methods that can be used to determine the height of the PBL top z_i are discussed. These methods are illustrated for an idealized profile of an atmospheric quantity in Figure 2.4. The top of the PBL is 1050 m in this case.

1. Gradient method

   In this frequently applied search algorithm, changes in the vertical profile of a trace substance (aerosol, water vapor) are interpreted as indications for an air-mass change with height. The first significant gradient is interpreted as the top of the PBL (Bösenberg 2002). Fig. 2.4b shows the vertical derivative of the measured atmospheric quantity. A local minimum at a height of 1050 m indicates a strong gradient. This height is defined as the PBL top.

2. Variance method

   As described above, mixing takes place at the top of the PBL due to entrainment of free-troposphere or residual-layer air. This leads to a high variability

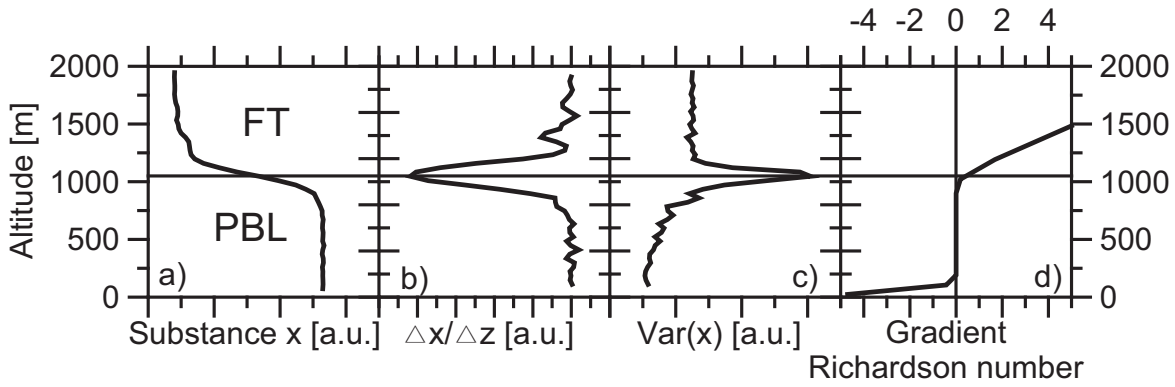

Figure 2.4: a) Idealized profile of an atmospheric quantity within the PBL and the free troposphere (FT) and the corresponding profiles of b) the gradient method, c) the variance method, and d) the gradient Richardson number.

of the measured atmospheric quantity in the transition zone, because alternating characteristics of free-troposphere and PBL air are observed. The height at which the variability takes its maximum is interpreted as the PBL top height z_i (Menut et al. 1999). An example is shown in Fig. 2.4c. For the analysis of the variability the temporal variance of the measured atmospheric quantity is investigated. The maximum in variance can clearly be identified at 1050 m. During nighttime, under statically stable conditions, this method may fail because of the low exchange rate at the top of the PBL.

3. Gradient Richardson number scheme

   A different approach is to analyze the driving forces of turbulence. Therefore, the gradient Richardson number scheme can be used (Fay 2005). The gradient Richardson number is defined as (Stull 1988)

$$Ri = \frac{\frac{g}{\overline{\Theta_v}} \frac{\Delta \overline{\Theta_v}}{\Delta z}}{\left(\frac{\Delta \overline{\vec{v}}}{\Delta z} \right)^2}, \tag{2.6}$$

   whereas $\overline{\vec{v}}$ is the mean horizontal wind vector. Eq. (2.6) is the ratio between the gradient form of the buoyancy term [see Eq. (2.4)] and the negative value of the shear term [Eq. (2.5)] of the TKE budget equation (2.3) under the assumption of horizontal homogeneity and by neglecting subsidence.
   According to Fig. 2.2, turbulence can be thermally driven, mechanically driven,

or it can be a mixture of both. Negative values of Ri indicate free convection, small positive values forced convection, and large positive values turbulence-free conditions. Therefore, a critical Richardson number Ri_c between 0.25 and 10 is defined to detect the transition from laminar to turbulent flows and vice versa. Then the top of the PBL is the height where flow characteristics change first from turbulent to laminar. This is shown in Fig. 2.4d. By assuming $Ri_c = 0.38$, the first transition from a turbulent flow to a laminar flow is detected at 1050 m. In contrast to the variance method, this technique can be applied to observations with low temporal resolution such as radiosonde profiles of temperature, water vapor, and wind vector. This method is also applied to identify the PBL top in numerical weather prediction models.

Chapter 3

Automated lidar observations

Automated observations with the Raman lidar Polly are used in this work for the analysis of the PBL top height at Leipzig. In the following, a short introduction into the basic lidar background is given, followed by a description of the Raman lidar Polly and the applied measurement strategy.

3.1 Lidar principle and equation

A lidar is an active remote-sensing instrument that makes use of the effects of atmospheric scattering and extinction to gain information on the state and composition of the atmosphere. Lidar is the acronym for **li**ght **d**etection **a**nd **r**anging. In principle, a lidar system consists of a transmitting and a receiving unit. Usually, the transmitter is a laser that emits pulses of monochromatic and almost coherent light. The receiver consists of a telescope which collects the backscattered light and a detector which counts the received photons. The distance z between the telescope and scattering volume can be calculated with the speed of light c and the time t between the emission of the laser pulse and the detection of the returned light:

$$z = \frac{tc}{2}. \tag{3.1}$$

The received power due to elastic scattering at the emission wavelength λ can be described with the lidar equation:

$$P(z,\lambda) = P_0 \frac{O(z)}{z^2} C_s(\lambda) \beta(z,\lambda) \exp\left[-2\int_0^z \alpha(z,\lambda)\mathrm{d}r\right]. \tag{3.2}$$

The power P received from range z depends on the emitted power P_0, the overlap function $O(z)$, a height-independent system constant $C_s(\lambda)$, the backscatter coefficient

$\beta(z, \lambda)$, and the extinction coefficient $\alpha(z, \lambda)$.
$O(z)$ describes the overlap between the laser beam and the field of view of the receiver. Close to the lidar there is no overlap and thus $O(z)$ is zero. The distance at which a complete overlap is achieved and $O(z)$ becomes 1 depends on the individual lidar system. Values vary between a few tens of meters and several thousand meters. $C_s(\lambda)$ represents the wavelength-dependent system efficiency. It contains all information about the performance of the individual system components (size of the telescope area, efficiency of detectors etc). $\beta(z, \lambda)$ is the scattering coefficient for the scattering angle of 180° and has the dimension of $\mathrm{m}^{-1}\mathrm{sr}^{-1}$. The exponential term describes the attenuation of light by scattering and absorption on its way through the atmosphere. According to the Lambert–Beer–Bouguer law, it depends on the volume extinction coefficient $\alpha(z, \lambda)$ and the length of the light path, which is in case of lidar twice the distance between the instrument and the backscattering volume. $\alpha(z, \lambda)$ is given in m^{-1}. Since scattering and extinction of molecules and particles is independent of each other, the corresponding coefficients can be split in a molecular and particle part:

$$\alpha = \alpha_{\mathrm{mol}} + \alpha_{\mathrm{par}} \tag{3.3}$$

and

$$\beta = \beta_{\mathrm{mol}} + \beta_{\mathrm{par}}. \tag{3.4}$$

3.2 Polly

Polly (**Po**rtab**l**e **l**idar s**y**stem; Engelmann 2003, Rhone 2004) is a small Raman lidar, that performs automated long-term observations. With a Raman lidar the inelastic backscatter signal caused by vibrational-rotational Raman scattering from nitrogen is measured in addition to the elastic backscatter signal and used to derive the extinction coefficient independently of the backscatter coefficient. For the determination of the PBL top height this application is not needed and therefore not further explained here. More details can be found in literature (Weitkamp 2005).
Figure 3.1a shows the optical setup of Polly. The frequency-doubled Nd:YAG laser emits light pulses of 120 mJ with a repetition rate of 15 Hz at a wavelength of 532 nm. A lens telescope expands the beam by the factor of eight to a diameter of about 50 mm. The laser divergence is reduced to less than 0.5 mrad. Via two mirrors the light pulses are transmitted into the atmosphere.
The backscattered light is collected with a Newtonian telescope. The main mirror has a diameter of 200 mm. The focal length of the telescope is 800 mm. An adjustable iris serves as a field stop and limits the field of view to 1.25–3.75 mrad. A lens

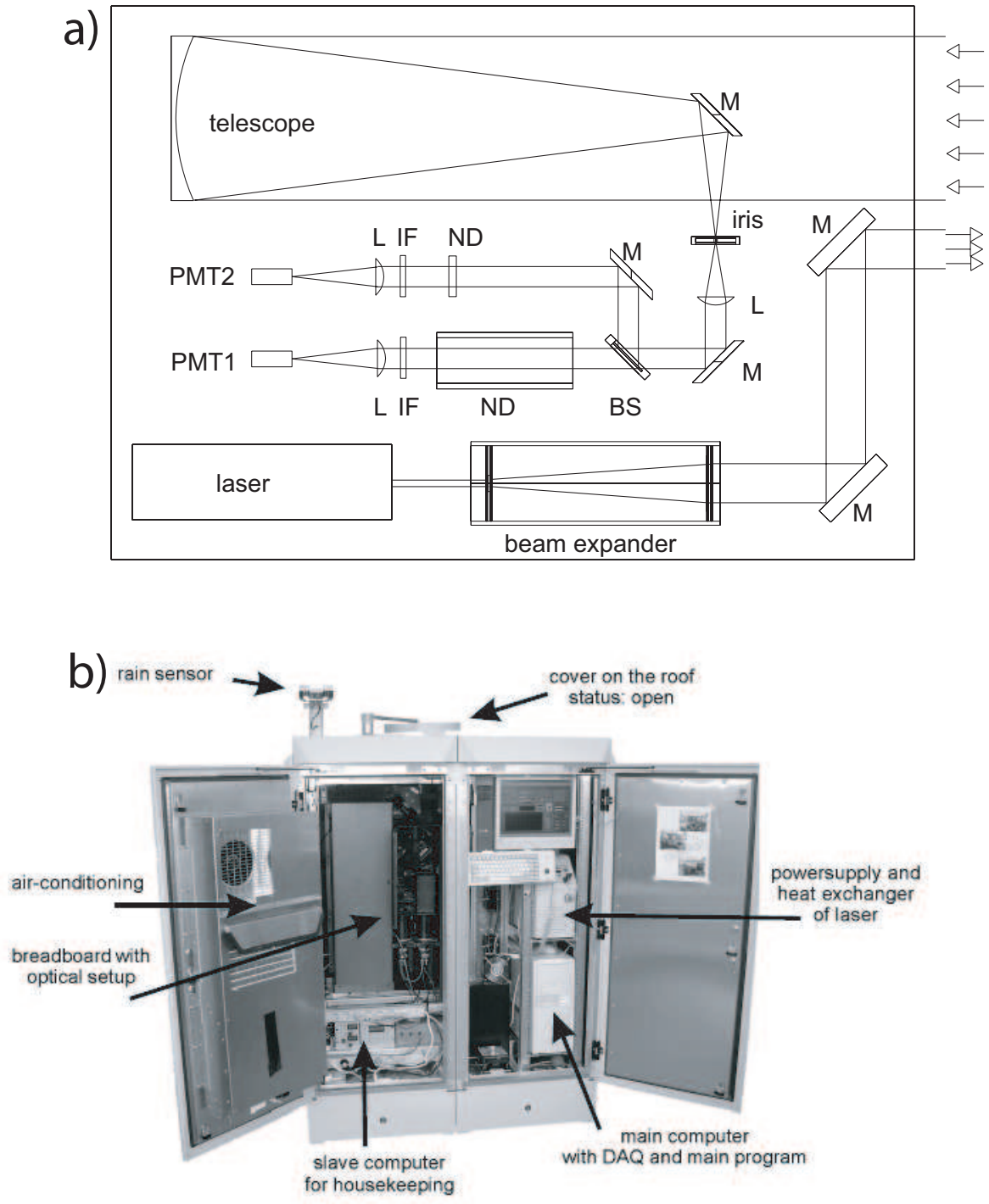

Figure 3.1: a) Schematic optical setup of Polly, M–mirror, L–lens, PMT–photomultiplier, ND–neutral density filter, BS–beamsplitter, and IF–interference filter. b) Photograph of Polly.

Table 3.1: Daily measurement program for Polly. Time is given in UTC.

Time	Time
00:01-02:14	12:01-14:14
03:08-03:13	15:08-15:13
04:08-04:13	16:08-16:13
05:08-05:13	17:08-17:13
06:08-06:13	18:08-18:13
07:08-07:13	19:08-19:13
08:08-08:13	20:08-20:13
09:08-09:13	21:08-21:13
10:08-10:13	22:08-22:13
11:08-11:13	23:08-23:13

collimates the light before the photons backscattered at 532 and 607 nm (the wavelength of vibrational-rotational Raman scattering from nitrogen) are separated with a beamsplitter. After passing a neutral-density filter, an interference filter, and a focusing lens, the photons in each channel are detected with a photomultiplier working in photon-counting mode. Signals are recorded with a range resolution of $\Delta z = 37.5$ m. Averaged profiles of 450 shots are stored.

The lidar is installed in a weatherproof cabinet, see Fig. 3.1b. An air-conditioning system and a rain sensor combined with a movable roof allow automatic measurements without supervision. Data analysis is also automatically performed on the measurement computer. A sensor for pressure and temperature at the cabinet provides atmospheric ground data for the data processing. Standard atmospheric conditions are assumed in these automated data analysis procedures in order to estimate the contribution of Rayleigh scattering and backscattering to the measured signals. Because of the incomplete laser-beam receiver-field-of-view overlap in the near range of the lidar, data coverage starts at a height of 180–400 m (depending on, e.g., the temperature stability within the cabinet or the adjustment of the laser beam after maintenance work).

Polly is run routinely at the site of the IfT in Leipzig since 1 August 2005. Measurements are taken daily from 00:01 to 02:14 UTC and from 12:01 to 14:14 UTC. Additionally, five minute long measurements are performed every hour since 20 January 2006 to measure the temporal development of the PBL throughout day and night. An overview of the measurement program is given in Table 3.1.

Chapter 4

PBL top detection methods

Several aerosol lidar methods have been developed for determining the PBL top height z_i. They are discussed in the following in detail. All methods are applied to the range-corrected signal which is more or less a measure for the particle backscatter coefficient, because extinction and molecular backscattering can be usually neglected for this application (Bösenberg and Linné 2002). The different methods are compared in Chapter 6 on the basis of several case studies. For the statistical analysis presented in Chapter 7, the modified wavelet covariance transform method is used.

4.1 Wavelet covariance transform

The wavelet covariance transform (WCT) technique after Brooks (2003), with modifications discussed below, is implemented in the Polly data analysis software for an automated finding of the PBL top height z_i. The WCT is defined as

$$W_f(a,b) = \frac{1}{a}\int_{z_b}^{z_t} f(z)h\left(\frac{z-b}{a}\right)\mathrm{d}z, \tag{4.1}$$

with the Haar function

$$h\left(\frac{z-b}{a}\right) = \begin{cases} +1, & b-\frac{a}{2} \le z \le b, \\ -1, & b \le z \le b+\frac{a}{2}, \\ 0, & \text{elsewhere.} \end{cases} \tag{4.2}$$

$f(z)$ in Eq. (4.1) is the range-corrected lidar backscatter signal $P(z)z^2$. z_b and z_t are the lower and upper limits of the profile, respectively. The step function $h\left(\frac{z-b}{a}\right)$ is illustrated in Fig. 4.1.

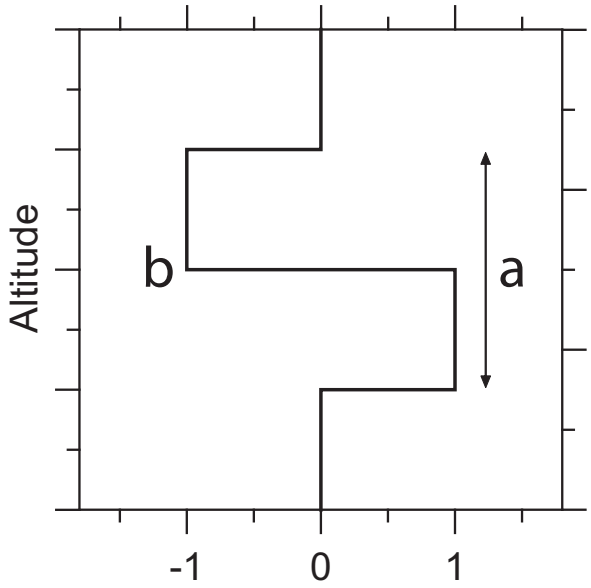

Figure 4.1: Shape of the Haar function.

The covariance transform $W_f(a, b)$ is a measure of the similarity of the range-corrected lidar backscatter signal and the Haar function. In the case of a clear lidar profile signature (see Fig. 4.2a) with high backscatter in the PBL and a low signal in the free troposphere (almost ideal step-like profile), $W_f(a, b)$ takes a local maximum at the height of the PBL top for $a = 12\Delta z = 450$ m (see Fig. 4.2b). Because the dilation a, the extent of the step function, is chosen *a priori*, the wavelet covariance transform is a function of the translation b, which is the location of the step.

As mentioned, the dilation a is chosen *a priori*. This parameter is important for a successful determination of z_i by the WCT. The ideal dilation is as large as the transition zone. For rather small values of a, signal noise dominates the vertical profile of W_f as can be seen for $a = 2\Delta z = 75$ m in Fig 4.2b. On the other hand, a too large dilation leads to a cut-off of the lower and upper parts of the profile, which is critical for the detection of a shallow PBL. This is shown in Fig. 4.2b for $a = 80\Delta z = 3000$ m. The lower and upper 1500 m of the profile are cut off due to the large dilation. The resulting profile of W_f is rather unrepresentative, because of the loss of information from lower heights. Thus, no clear peak can be identified.

In addition, if the atmosphere contains multiple particle layers, see Fig. 4.3a, these small-scale structures may not be resolved, when the dilation is too small or too large. In Fig. 4.3b, the optimum dilation value is $a = 12\Delta z = 450$ m. As a consequence, the PBL top determination is rather uncertain in such cases. The selection of an

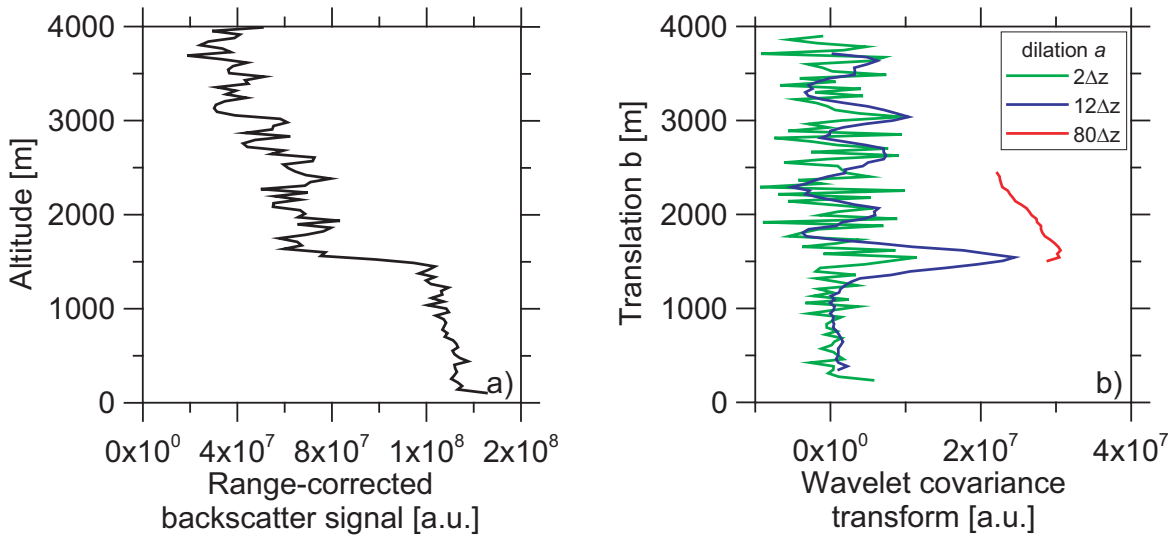

Figure 4.2: Lidar measurement on 28 July 2006, a) range-corrected signal, b) corresponding WCT for various dilations a.

appropriate value of the dilation a is the main challenge for a successful retrieval of the PBL top height with this method.

Davis et al. (2000) tried to find the right dilation for airborne lidar measurements by calculating the wavelet variance defined by Gamage and Hagelberg (1993):

$$D^2(a) = \int_{z_t}^{z_b} W_f(a,b)\mathrm{d}b. \tag{4.3}$$

The location of the global maximum of this function is chosen to be the optimum dilation. Unfortunately, this method cannot be used in the case of Polly data evaluation. The lack of data because of the incomplete laser-beam receiver-field-of-view overlap at lower altitudes leads to rather unsatisfying solutions for the dilation a. In addition, instrumental noise and cloud fields have a strong influence on the wavelet variance and thus also on the choice of a with this method.

Brooks (2003) developed an iteration method that is applicable to observations of stable maritime planetary boundary layers. The approach starts with an arbitrary large dilation. Then the full width at half maximum of $W_f(b)$ is chosen to be the new dilation. This iteration goes on until the dilation a does not change anymore.

We found that this method often fails when cloud fields are present and in situations with multiple aerosol layers. During the transition period from nighttime to daytime boundary-layer conditions (see Sec. 2.3) with rapid temporal changes in the lidar profiles and a complex aerosol layer structure (PBL and RL), the iteration method fails completely. Thus, we were forced to introduce several modifications that allow us

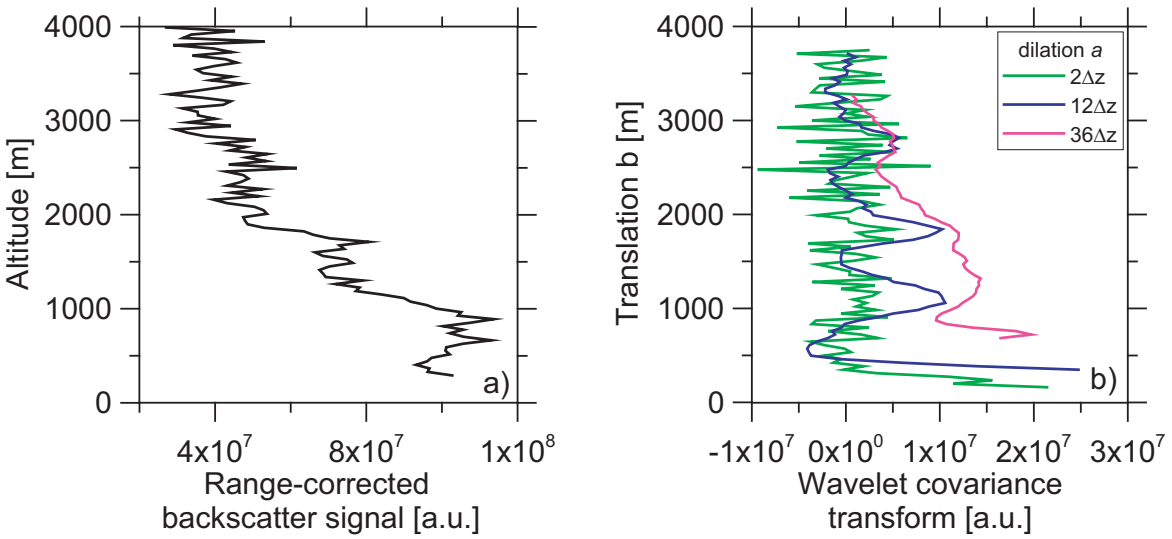

Figure 4.3: Lidar measurement on 12 August 2006, a) range-corrected signal, b) corresponding WCT for various a.

to determine the PBL top height z_i even under conditions with clouds and multiple aerosol layers.

4.2 Modifications on the WCT method

4.2.1 Threshold value of the WCT

The PBL top height is frequently indicated by the first strong gradient above ground. A threshold value for the waveform covariance transform is thus introduced that allows us to identify a significant gradient and to omit the weak gradients. Equation (4.1) can be split up as follows:

$$\begin{aligned} W_f(a,b) &= \frac{1}{a}\int_{z_b}^{z_t} f(z)h\left(\frac{z-b}{a}\right)dz \\ &= \frac{1}{a}\int_{z_b}^{b-\frac{a}{2}} f(z)h\left(\frac{z-b}{a}\right)\mathrm{d}z + \frac{1}{a}\int_{b-\frac{a}{2}}^{b} f(z)h\left(\frac{z-b}{a}\right)\mathrm{d}z \\ &+ \frac{1}{a}\int_{b}^{b+\frac{a}{2}} f(z)h\left(\frac{z-b}{a}\right)\mathrm{d}z + \frac{1}{a}\int_{b+\frac{a}{2}}^{z_t} f(z)h\left(\frac{z-b}{a}\right)\mathrm{d}z. \end{aligned} \tag{4.4}$$

Since the Haar function is 0 for $z_b \leq z < b - \frac{a}{2}$ and $b - \frac{a}{2} < z \leq z_t$, 1 for $b - \frac{a}{2} \leq z \leq b$, and -1 for $b \leq z \leq b + \frac{a}{2}$ it follows:

$$W_f(a,b) = \frac{1}{a}\left(\int_{b-\frac{a}{2}}^{b} f(z)\mathrm{d}z - \int_{b}^{b+\frac{a}{2}} f(z)\mathrm{d}z\right). \tag{4.5}$$

For a discrete lidar signal the dilation is defined as

$$a = n\Delta z,\ n = 2, 4, 6, 8... \tag{4.6}$$

and the position of the translation b has to be chosen in between two discrete data points to assure an equal number of data points in each integral. This leads to the discretized form of the WCT for $f(z) = P(z)z^2$:

$$\begin{aligned} W_f(a,b) &= \frac{1}{n\Delta z}\left(\sum_{b-\frac{a}{2}}^{b} P(z)z^2\Delta z - \sum_{b}^{b+\frac{a}{2}} P(z)z^2\Delta z\right) \\ &= \frac{1}{n}\left(\sum_{b-\frac{a}{2}}^{b} P(z)z^2 - \sum_{b}^{b+\frac{a}{2}} P(z)z^2\right), \end{aligned} \tag{4.7}$$

what can be separated into mean values above and below the height of the translation b, each with an extent of $\frac{a}{2}$:

$$\begin{aligned} W_f(a,b) &= \frac{1}{n}\left(\sum_{b-\frac{a}{2}}^{b} P(z)z^2 - \sum_{b}^{b+\frac{a}{2}} P(z)z^2\right) \\ &= \frac{1}{2}\left(\overline{P(z)z^2}^{\text{below}} - \overline{P(z)z^2}^{\text{above}}\right) = \frac{1}{2}\Delta\left(\overline{P(z)z^2}\right). \end{aligned} \tag{4.8}$$

In the next step, we normalize the range-corrected signal by its maximum value found below 1000 m. This is usually the maximum value of $P(z)z^2$ within the PBL. The normalization guarantees the applicability of the threshold method on very different backscatter conditions in rather clean or very polluted air. An example of a normalized signal and the corresponding WCT is presented in Fig. 4.4a and b, respectively. $W_f(a,b)$ takes a clear local maximum with a value of 0.12 for the translation $b = b_{\max} = 1900$ m which corresponds to the height of the PBL top. According to Eq. (4.8), a value of 0.12 shows a decrease of the mean signal of 24% with respect to the maximum value in the PBL:

$$W_f(a, b_{\max}) = 0.12 = \frac{1}{2}\Delta\left(\overline{P(z)z^2}\right) = \frac{1}{2}(0.24). \tag{4.9}$$

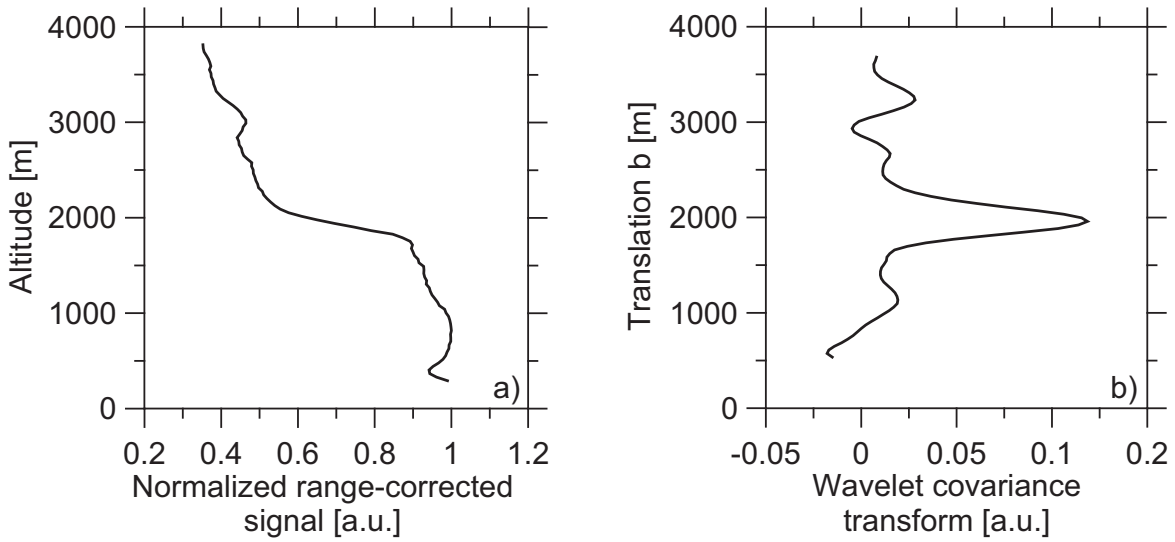

Figure 4.4: a) Normalized range-corrected signal on 12 June 2006, b) corresponding WCT for $a = 12\Delta z$.

Now, a threshold for $W_f(a, b)$ can be introduced. If no significant gradients are found below and above the transition zone, this value is also independent of the value of the dilation a itself. A threshold value of 0.05 was found to work well. According to Eq. (4.9), this means that already a decrease of the mean signal of 10% percent with respect to the maximum PBL value is sufficient to identify the PBL depth. The first height above ground at which a local maximum of $W_f(a, b)$ occurs, that exceeds the threshold value of 0.05 is defined as the PBL top height z_i. If the threshold condition is not fulfilled, a PBL top is not provided as output in the algorithm.
In Fig. 4.4b the PBL top height is calculated to 1959 m by this method. The step in the normalized range-corrected signal at around 1000 m is obviously not significant. The corresponding local maximum of $W_f(a, b)$ has a value of about 0.025, which is well below 0.05. This step is therefore not considered for the PBL top detection.

4.2.2 Cloud detection

Clouds are characterized by a steep increase of the range-corrected lidar signal at the cloud base followed by a strong decrease of the signal with increasing cloud penetration depth. In Fig. 4.5a such a cloud signal with a cloud base at about 1400 m is presented. Because of this characteristic signal shape, the WCT can be used for detecting clouds. For the already given example, the WCT is shown in Fig. 4.5b. Due to the definition

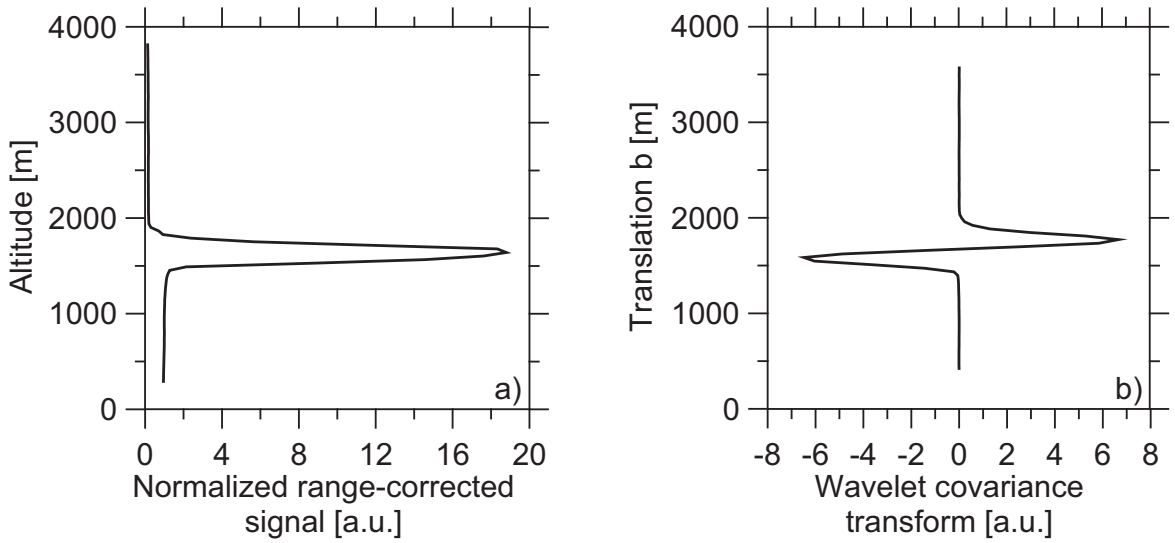

Figure 4.5: a) Normalized range-corrected signal on 10 June 2006, b) corresponding WCT for $a = 6\Delta z$.

of the Haar function, $W_f(a, b)$ has a characteristic shape as well. It becomes negative at the cloud base and shows a local minimum before it becomes positive with a local maximum. Thus, the cloud can be identified with the help of a negative threshold. It was found that cloud detection works very well for a threshold of -0.1 and for a dilation of $a = 6\Delta z = 225$ m. The cloud base is then defined at the height point below the altitude where $W_f(a, b)$ first falls below the chosen threshold value. The cloud base in Fig. 4.5 is identified with this method at 1397 m.
If a cloud is detected in the lidar profile, the corresponding height is used as a cut-off and only values below the cloud base are used for the determination of the PBL top. If no significant gradient can be detected, it is very probable that this cloud has formed within the PBL. In that case, no PBL top height is provided.

4.2.3 Height-dependent dilation

As described above, the choice of a proper dilation a is important. The selection of a fixed dilation $a = 12\Delta z$ worked very well except for cases with very shallow PBL and very extended transition zones. Our experience shows that the use of a dilation profile $a(z)$ described by a quadratic increase of the dilation with height (see Fig. 4.6) is a good compromise to detect very low PBL top heights with usually very narrow transition zones, but also to identify extended transition zones (usually observed at heights above 500 m).

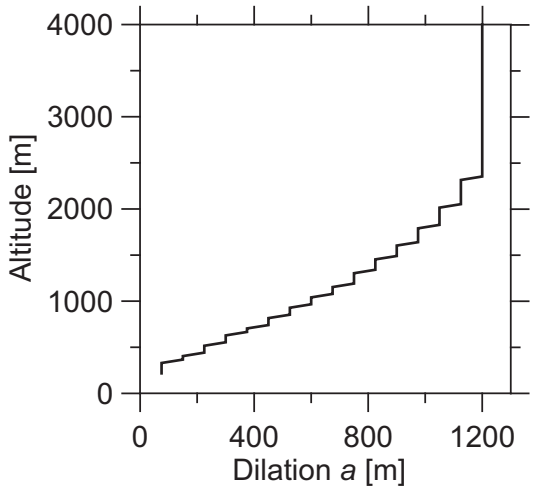

Figure 4.6: Example of an height-dependent dilation; a quadratic increase with height is shown.

An example is given for the morning hours on 12 September 2006. The range-corrected signal (Fig. 4.7a) shows a developing PBL with a depth of about 350 m and a RL with its top at about 760 m with an extended transition zone.
The corresponding WCT for three dilation options (Fig. 4.7b) shows that the low PBL top (close to the detection minimum of 250 m) can be identified with the height-dependent dilation method and for $a = 2\Delta z = 75$ m. For $a = 10\Delta z = 375$ m a detection is not possible due to the cut-off of the lower part of the lidar signal profile and the resulting non-existence of a peak in $W_f(a, b)$ at the corresponding height.
On the other hand, $W_f(2\Delta z, b)$ does not exceed the threshold value of 0.05 at the RL top height, whereas $W_f(10\Delta z, b)$ has a clear peak with a value of 0.08 at this height. The WCT with the height-dependent dilation can also be used to identify the RL top. If one considers that the shape of the RL in the lidar signal profile in this case could represent a PBL in another case, it can be concluded that the height-dependent dilation method works best to detect various PBL tops.

4.3 Other techniques for PBL top detection

The general ideas of the methods described below were already discussed in Section 2.4. In the following, the application to lidar profiles is explained.

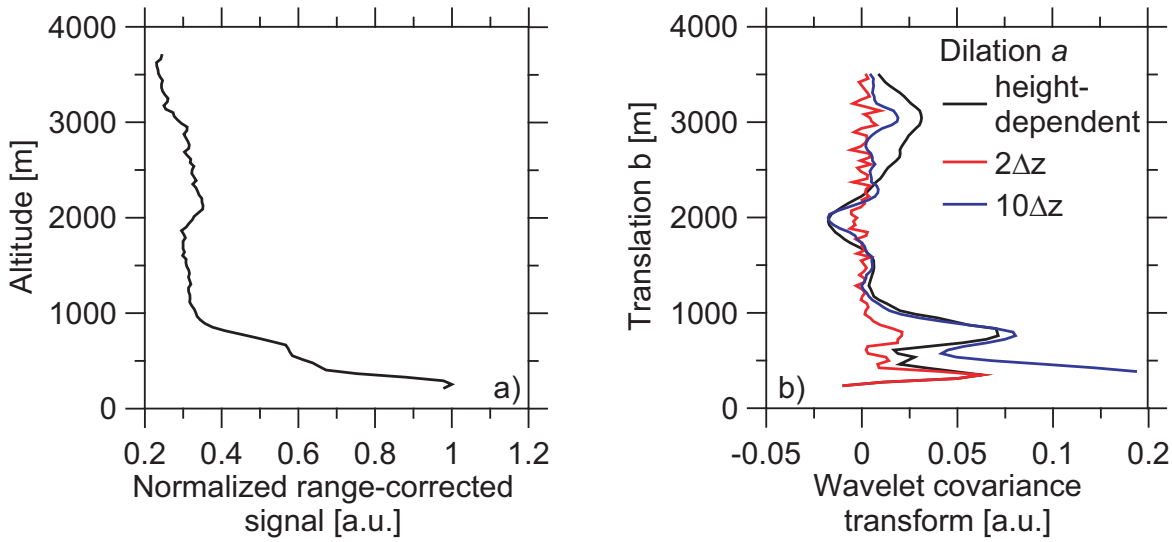

Figure 4.7: a) Normalized range-corrected signal on 12 September 2006, 09:08–09:23 UTC, b) corresponding WCT for different dilation options.

4.3.1 Gradient method

The gradient method is sometimes also referred to as inflection-point method (Menut et al. 1999) and has already been illustrated in Section 2.4. The height at which the first derivative of the range-corrected signal

$$\frac{\mathrm{d}}{\mathrm{d}z}\left(P(z)z^2\right) \tag{4.10}$$

takes its minimum is defined as the PBL top height z_i. Because this method suffers strongly from noise, vertical averaging is needed. An alternative way for deriving the slope of $P(z)z^2$ is to calculate a linear fit with a certain number of points.

4.3.2 Variance method

The variance method, also called centroid method (Menut et al. 1999), has also been described in Sec. 2.4. The PBL top height z_i is that height at which the temporal variance

$$Var(z) = \frac{1}{K}\sum_{k=1}^{K}\left(P(z)_k z^2 - \overline{P(z)z^2}\right)^2 \tag{4.11}$$

takes its maximum. Because a large number of vertical profiles is needed to calculate $Var(z)$, the temporal resolution in the determination of z_i is limited.

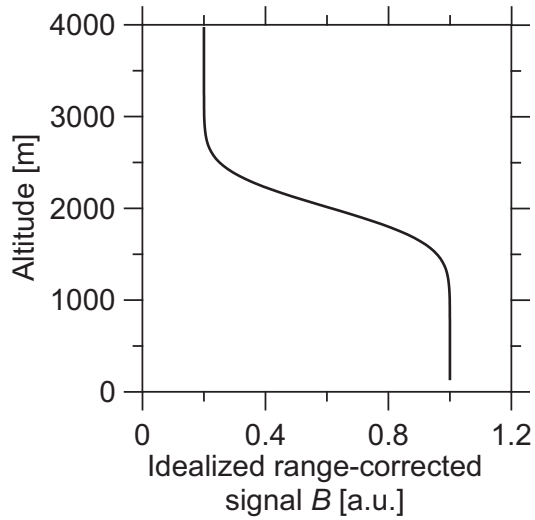

Figure 4.8: Example of an idealized backscatter profile with $z_i = 1900$ m, $d = 450$ m, $B_m = 1$, and $B_u = 0.2$.

4.3.3 Fitting method

A recent approach (Steyn et al. 1999) has been made by fitting an ideal backscatter profile to the real profile to determine the midpoint and the extent of the transition zone. The artificial profile is defined as

$$B(z) = \frac{B_m + B_u}{2} - \frac{B_m - B_u}{2} erf\left(\frac{z - z_i}{d}\right), \tag{4.12}$$

where B_m and B_u are mean coefficients of the ideal backscatter profile in and above the PBL, respectively, erf describes the error function and d is related to the thickness of the transition zone. An example of an artificial profile is shown in Fig. 4.8.
The artificial profile is compared with the measured profile by calculating the root mean square (RMS). This leads to a 4-dimensional field of RMS depending on z_i, d, B_m, and B_u. The parameters for which the RMS field has an absolute minimum are chosen to be the best fitting ones. The value of the corresponding z_i is defined to be the PBL top height. The advantage of this method is that beside the PBL top height also information on the extent of the transition zone can be achieved by analyzing the parameter d.

Chapter 5

Additional data sources

In this work, automated observations with the Raman lidar Polly are analyzed and compared with model results (Lokal-Modell of the DWD) regarding PBL top heights. On special days with pronounced PBL evolutions, radiosondes were launched and the Doppler wind lidar WiLi for vertical wind observations was run in addition. In the following, a short description of these additional data sources is given.

5.1 PBL top height determined with the Lokal-Modell

PBL top heights as calculated with the Lokal-Modell (LM) are provided by the DWD with a resolution of 1 hour. Since 2000 the LM is in operational use. The mixing height, i.e., the height of the layer of active mixing, is calculated. This height is denoted PBL top height in the following. The PBL top height is provided as input for several dispersion models. The algorithm to derive the PBL depth was developed to support, e.g., the radioactivity emergency system RODOS (**R**ealtime **o**nline **d**ecisi**o**n **s**upport system for nuclear emergency management in Europe).
The gradient Richardson number scheme described above is used to derive the PBL top from the model output. Forecasts are provided two times per day for 48 h in 1 h intervals based on the analysis at 00:00 and 12:00 UTC. The critical Richardson number Ri_c is set to 0.38 (Fay et al. 1997). Starting at the ground, the altitude of the first transition from turbulent to laminar flow is defined as the PBL top height. To reach the exact value of 0.38 an interpolation between two model layers is made which leads to an interpolated height.
Based on validation campaigns it has been found that the PBL top height is system-

atically underestimated by approximately 10% to 20%. During convective situations or periods with frontal passages an underestimation of 30% has been observed (Fay 1998). Episodes of strong inversions in winter may often not allow the computation of the PBL top height. Nighttime values were found to be usually not reliable.
Because dispersion models need a full set of PBL top heights throughout the day, the following constraints have been implemented:

- The height of the PBL top is only calculated from the first full hour after sunrise until the last full hour before sunset. At nighttime a standard value depending on the orography is set; for Leipzig this value is 389 m.

- The minimum of the PBL top height is 200 m. If lower values are computed, e.g., in cold winter nights, these values are replaced by $z_i = 200$ m.

- If no PBL top is found below 3000 m or if the atmosphere is non-turbulent up to model level 36 (ca. 214 m) a default value is computed. In this case, the PBL top height is calculated as the height difference between model level 28 and 35, e.g., 1243 m for 1000 hPa ground pressure in Leipzig.

In this work, PBL tops derived from the 00:00 and 12:00 UTC analysis plus the corresponding 11–hour forecast are used. Values of 200 m and 389 m are mostly neglected, because they have no meteorological background and are only provided as input for dispersion models.

5.2 Auxiliary observations

5.2.1 WiLi

For measurements of vertical wind speeds IfT's coherent Doppler lidar was used. This system has a vertical resolution of 75 m. The measurements start at 400 m height. The emitted laser pulse has an energy of 1.5 mJ at 2022.5 nm wavelength, which corresponds to a minimum of the atmospheric water-vapor absorption spectrum. The repetition rate is 750 Hz. Measurements are made with 5 and 30 s resolution. The heterodyne detection scheme allows one to measure line-of-sight wind speeds in the PBL up to 20 m/s with a resolution of 0.1 m/s. Further details are given in Engelmann et al. (2007), Engelmann (2003), and Rhone (2004).

5.2.2 Radiosonde

On special days Vaisala RS-80 radiosondes were launched at the IfT site. They provide geopotential height, temperature ϑ (°C), and relative humidity RH at the pressure levels. From these quantities, the water-vapor-to-dry-air mixing ratio and the virtual potential temperature are calculated [e.g., Liljequist and Cehak (1979), Garratt (1992)]. Additionally, radiosonde data from the DWD site at Oppin, 40 km northwest of Leipzig, have been used (these data are provided by the University of Wyoming at http://weather.uwyo.edu/upperair/sounding.html).

Chapter 6

Case studies

In this chapter, the achievements and limits of the methods described in Chapter 4 are analyzed by applying them to Polly data for several measurements periods. PBL top heights computed with the LM (Sec. 5.1) are used for comparison. The wind lidar WiLi and radiosondes (Sec. 5.2) were used to investigate the convective state of the atmosphere. The diurnal variation of the PBL is analyzed as well.

6.1 11–13 September 2006

From 11–13 September 2006 an intensive measurement campaign took place at the IfT site in Leipzig. Polly and WiLi measured at the same time and radiosondes were launched. A high-pressure system over eastern Europe (Fig. 6.1) dominated the weather in Germany for the whole period. The observed days were characterized by cloud-free conditions and, as Figure 6.2 indicates, by remarkably constant meteorological conditions. Daily minimum and maximum temperatures increased only slightly from 11 to 13 °C and 28 to 29 °C, respectively.
Fig. 6.3a shows the evolution of the range-corrected signal on 11 September 2006. A typical PBL evolution as described in Section 2.3 was observed. Fig. 6.3b shows the vertical wind speeds determined with the wind lidar WiLi. Yellow and red colors indicate updrafts, green and blue colors downdrafts. Sunrise was at 04:38 UTC and sunset at 17:38 UTC. A growing convective PBL can be identified shortly after 06:00 UTC. The RL is completely mixed into the convective PBL at about 11:00 UTC. The maximum depth of the PBL of 1172 m is reached at 15:00 UTC (Fig. 6.3a). The vertical wind observations in Fig. 6.3b indicate the convective period from 09:00 to 15:30 UTC with frequent up- and downdrafts. The radiosonde launches at 06:39 and 13:36 UTC (Fig. 6.3c and d) provide information about the thermodynamic state of

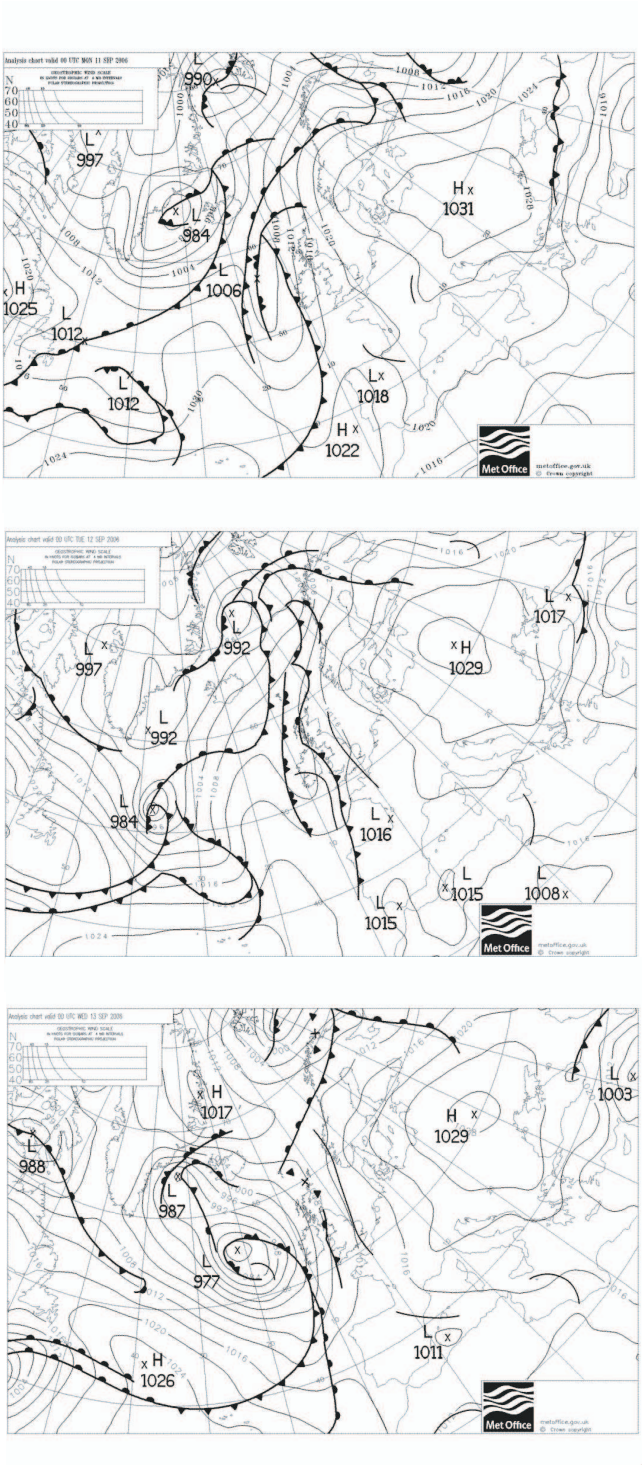

Figure 6.1: Analysis of ground pressure and fronts at 00:00 UTC on 11 (top), 12 (center), and 13 (bottom) September 2006 . The analysis maps were provided by the Met Office of the UK and were downloaded from http://www.wetterzentrale.com.

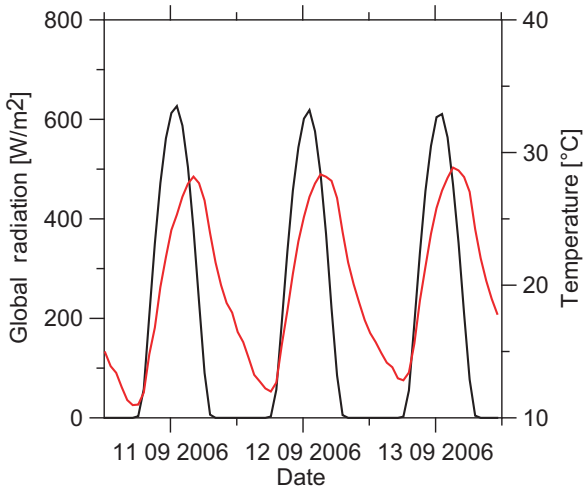

Figure 6.2: Global radiation (black line) and ground temperature (red line) observed at IfT on 11–13 September 2006.

the atmosphere. The profile of virtual potential temperature Θ_v of the first radiosonde launch shows a thin layer at the surface with constant values. The depth of this layer was approximately 100 m. Above this shallow layer, a strong positive gradient of Θ_v up to 1000 m was measured.

The buoyancy term BT (Eq. 2.3) in Fig. 6.3c and d is roughly estimated from the radiosonde data:

$$BT(z) = -K\frac{g}{\overline{\Theta_v}}\frac{\Delta\Theta_v}{\Delta z}. \tag{6.1}$$

For simplicity we assume 1 $\frac{\mathrm{m}^2}{\mathrm{s}}$ for the unknown K. Although horizontal wind information is not available, BT allows us to identify layers that differ with respect to the thermal production or loss of TKE. As can be seen in Fig. 6.3c, only the first value of BT above ground at 102 gpm is positive. This indicates a growing but still very shallow convective PBL. The statically stable layer above with strong negative values prohibited convective mixing in higher levels. The profile of the water-vapor-to-dry-air mixing ratio s shows a moist lower troposphere.

In the early afternoon the situation had changed (Fig. 6.3d). Convective mixing dominated up to 1000 m, as the almost constant values of Θ_v and s indicate. As can be seen in the profile of BT, thermal turbulence was generated at the surface (strong positive values) and suppressed at the top of the convective PBL at about 1000 m (strong negative values).

Fig. 6.4 shows the results regarding the detection of the PBL top height. Due to the incomplete laser-beam receiver-field-of-view overlap in the near range of the lidar, the

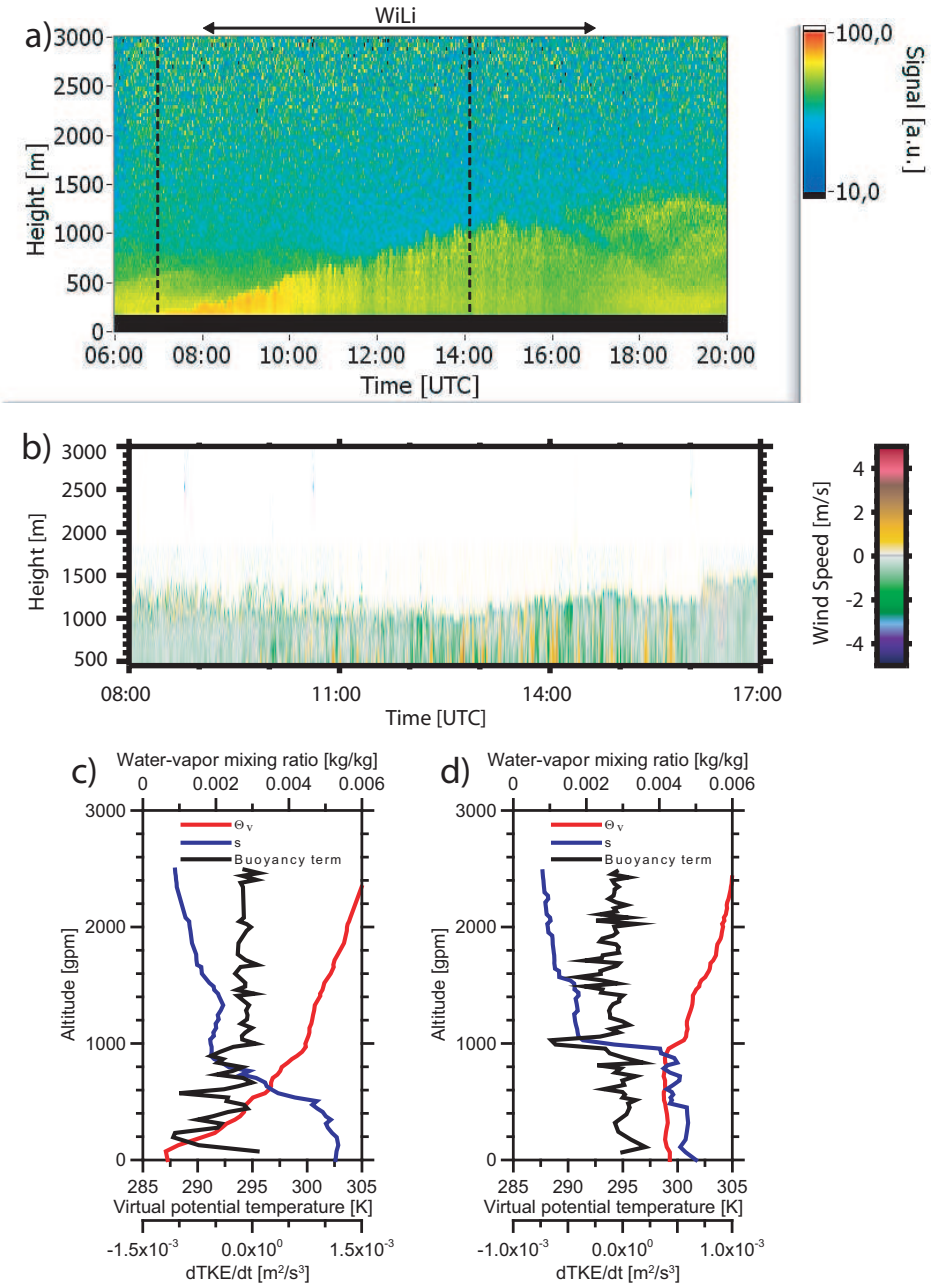

Figure 6.3: Evolution of the PBL observed with Polly, WiLi, and radiosondes on 11 September 2006. a) Range-corrected signal observed with Polly with 30 s and 37.5 m resolution, b) vertical wind observed with WiLi with 30 s and 75 m resolution, c) and d) radiosonde profiles of virtual potential temperature (red), water-vapor-to-dry-air mixing ratio (blue) and buoyancy term BT of Eq. (2.3) (black). Vertical dashed lines in a) indicate the launch time of the radiosondes at 06:39 and 13:36 UTC. The horizontal bar in a) indicates the WiLi measurement period.

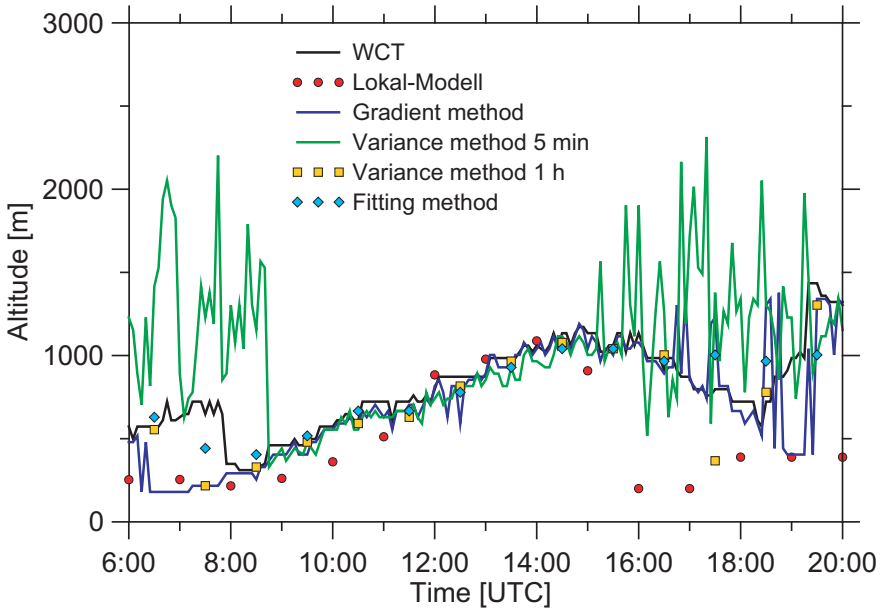

Figure 6.4: PBL top heights determined on 11 September 2006 by applying the WCT, gradient, variance, and fitting methods (Chapter 4). PBL top heights derived from the Lokal-Modell (LM) are also shown. Five-minute resolution is applied for the WCT, gradient, and variance methods. One-hour resolution is used for the fitting method and for a second retrieval with the variance method.

observation starts at 180 m height. Signals measured within 5 min are sufficient to determine the PBL top height with the WCT and the gradient method. The variance method was applied to average signal profiles of 5 and 60 min. Results of the fitting method are based on signal profiles measured within 60 min. In addition, PBL top heights as computed with the LM are shown.

As can be seen, a clear determination of the PBL top height is possible with all methods during the period of convective activity (see wind data in Fig. 6.3b) from 09:00–15:30 UTC. In the early morning (before 08:00 UTC), the late afternoon (after 16:00 UTC), and during night, the determination is critical because a clear separation of the PBL and the RL is obviously not possible. The 5-min variance method completely fails from 15:00–09:00 UTC. The WCT method and the fitting method identify the RL top and interpret it as PBL top height (e.g., before 08:00 UTC). The gradient method was obviously able to detect the PBL top already in the early morning (06:30–08:00 UTC). But as shown in Fig. 6.3c, the PBL was only of 100 m depth at 6:40 UTC. Thus, values for the PBL top height from the gradient method (minimum

180 m due to the incomplete overlap) are overestimated at the beginning of this time period. The LM sets the PBL top to a constant value of 389 m from 18:00–08:00 UTC and to 200 m from 16:00–17:00 UTC. One can conclude that the incomplete laser-beam receiver-field-of-view overlap in the near range of the lidar strongly affects the detection of the PBL top at nighttime and in the early morning. Nevertheless, Fig. 6.3 clearly demonstrates that an automated, accurate detection of the daytime PBL top height from continuous lidar observations is possible.

On 12 September 2006 a similar evolution of the PBL was observed (Fig. 6.5a). Again, radiosondes were launched in the early morning and in the early afternoon. A well-mixed layer was found again in terms of Θ_v and s in the afternoon. The strong negative value of BT at about 1150 m indicates the top of the PBL. According to the vertical-wind observations (Fig. 6.5b), the convective-mixing period lasted until 16:30 UTC on this day, and thus almost one hour longer than on 11 September 2006. All PBL top detection methods (Fig. 6.6) work well when applied to observations from 09:30–17:00 UTC. The full daytime evolution from 08:00 to 18:00 UTC is correctly determined with the WCT, the gradient, and the 1-h variance methods. The LM computed reasonable values for the period from 07:00–15:00 UTC and at 17:00 UTC. Again problems occur during late afternoon, at nighttime, and in the early morning.

On 13 September 2006 (Fig. 6.7) a lofted aerosol layer above the PBL was present, that is clearly visible in the wind plot. As on the days before, the early-afternoon radiosonde shows a well-mixed PBL. The lofted layer is characterized by another increase in the water-vapor mixing ratio. The optical depth of this layer was too low to influence the convective activity expressed by the strength of downdrafts and updrafts (see Fig. 6.7b).

The presence of the lofted layer complicates the PBL top height determination (Fig. 6.8). However, the WCT method is robust and works well throughout the period from 08:00–17:00 UTC. The 5-min variance method and the fitting method have the largest problems to resolve the daytime evolution of the PBL top height. The LM provides reasonable values before 10:00 UTC and from 12:00–15:00 UTC.

The PBL top heights determined with the 1-h variance method, the gradient method, and the fitting method and the values provided from the LM are directly compared to the PBL depths computed with the WCT technique in Fig. 6.9. Values measured on 11–13 September 2006 from 09:00-15:00 UTC are considered. The 5-min variance results are completely excluded because of the noise in the data.

As mentioned, all methods work well when a pronounced daytime evolution of the PBL is observed. Nevertheless, the fitting method and the LM underestimate the PBL top height systematically even under these almost ideal atmospheric conditions.

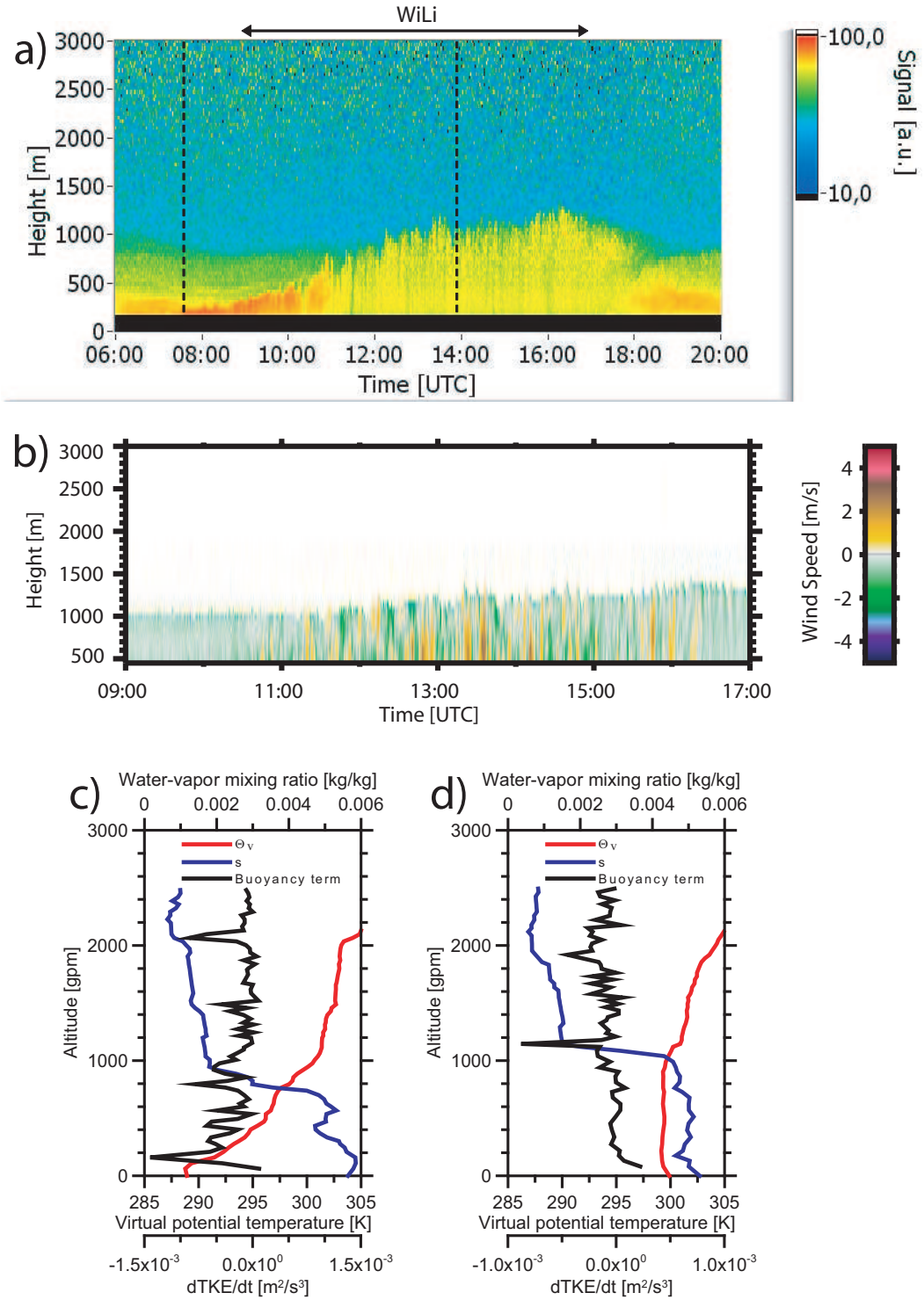

Figure 6.5: Same as Fig. 6.3, but for 12 September 2006. Radiosondes were launched at 06:58 and 14:05 UTC.

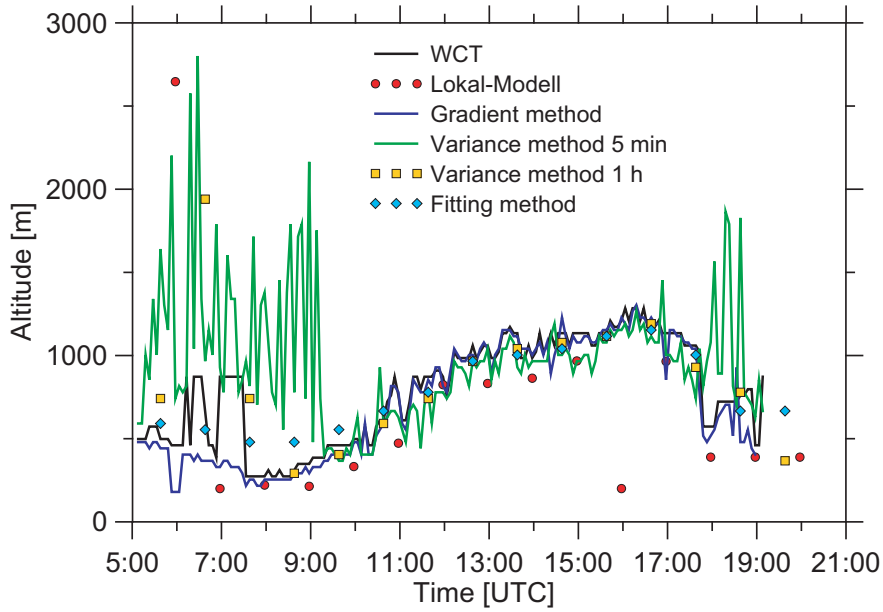

Figure 6.6: Same as Fig. 6.4, but for 12 September 2006.

The reason for the underestimation of the PBL depth with the fitting method is a non-negligible slope in the range-corrected signal within the PBL. This causes systematic errors in the fitting procedure.

6.2 3–5 July 2006

Another intensive measurement campaign was performed on 3–5 July 2006. A high-pressure system over eastern Europe and a low-pressure system over western Europe caused the advection of warm and humid air from southern Europe (Fig. 6.10). In contrast to the period of 11–13 September 2006, cumulus clouds formed at the top of the PBL (see Fig. 6.11, center). The PBL reached to heights of about 2 km in the late afternoon on 4 and 5 July 2006 (see Fig. 6.11 and 6.12). The vertical-wind observations in Fig. 6.12 indicate pronounced updrafts and downdrafts during daytime throughout the whole period. Fig. 6.13 presents the PBL top heights determined with Polly (WCT technique) and as computed with the LM. Data coverage of Polly started at 400 m height within this period. The most significant feature is the systematic underestimation of the PBL top height by the atmospheric simulation model on 3 and 5 July 2006. As can be seen in Fig. 6.14, the mean difference between the lidar and the LM values on these days was 270 m. The very complex parameterization of the turbulence, soil characteristics etc. makes is rather difficult to find specific reasons for

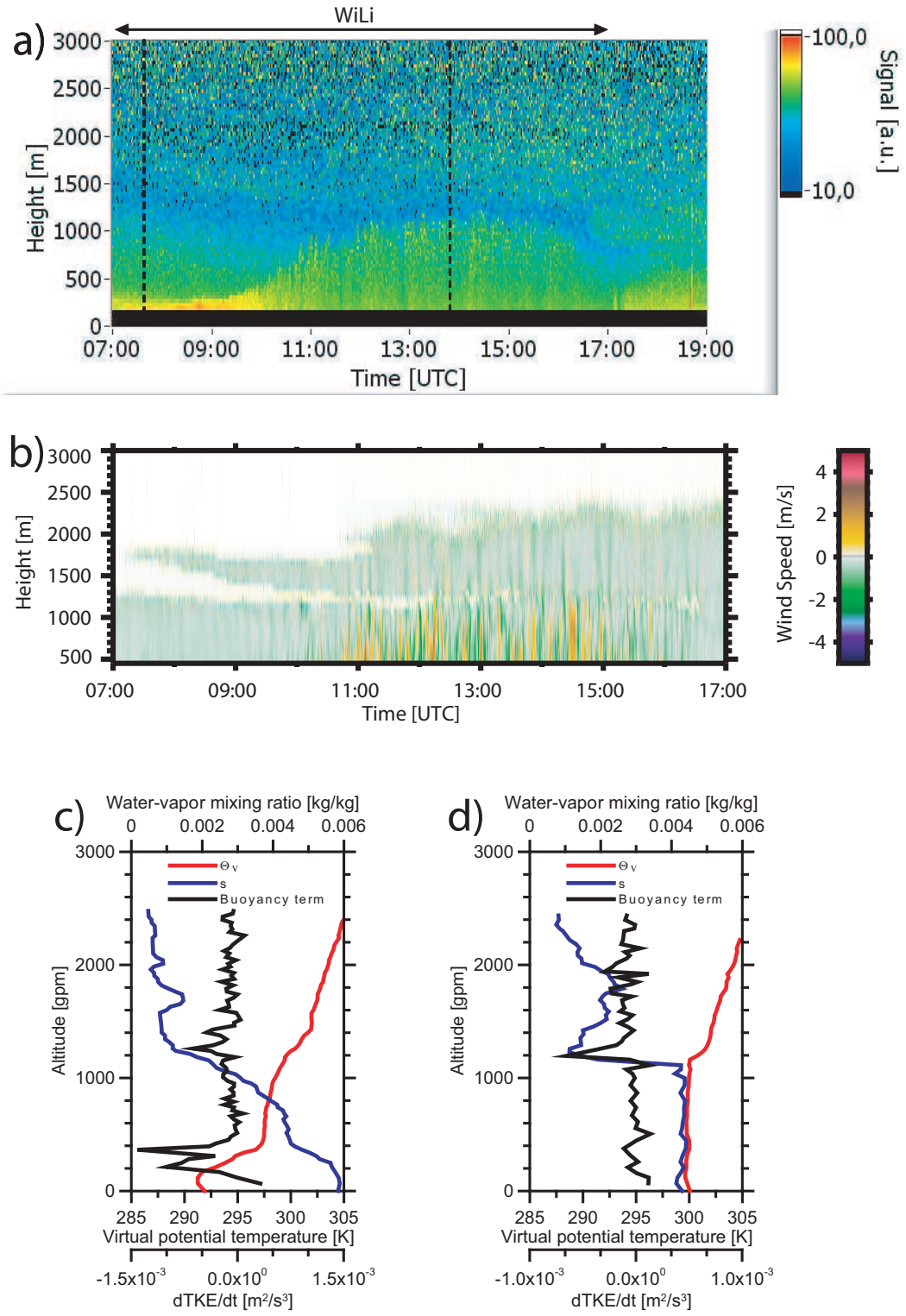

Figure 6.7: Same as Fig. 6.3, but for 13 September 2006. Radiosondes were launched at 07:37 and 13:50 UTC.

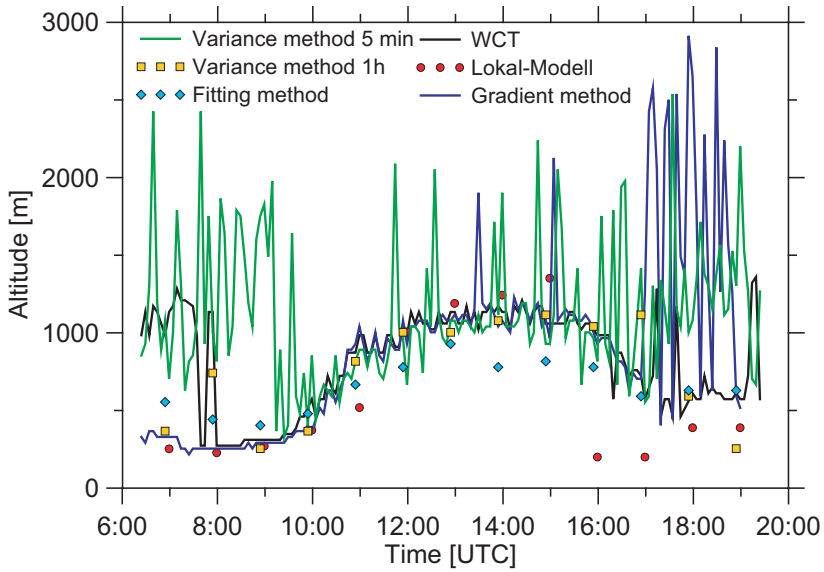

Figure 6.8: Same as Fig. 6.4, but for 13 September 2006.

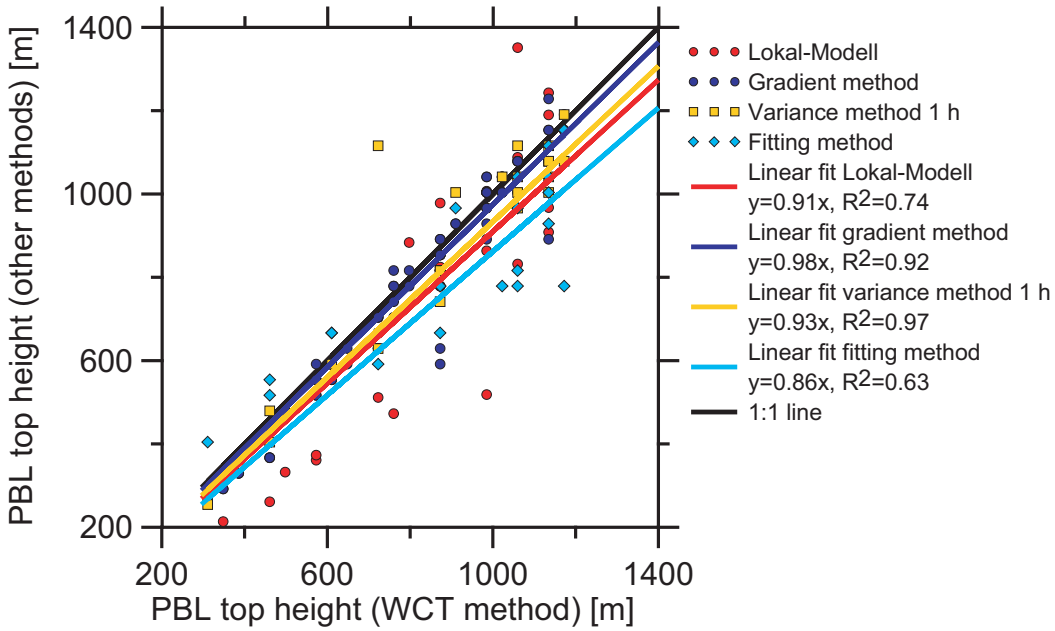

Figure 6.9: PBL top height determined with the 1-h variance method (yellow), the gradient method (dark blue), the fitting method (light blue), and as computed with the atmospheric model LM (orange) versus the PBL top height determined with the WCT method. Data from 11–13 September 2006, 09:00 to 15:00 UTC are considered. Linear regression lines are computed in addition. The respective equations and the quadratic correlation coefficient R^2 are given in the legend.

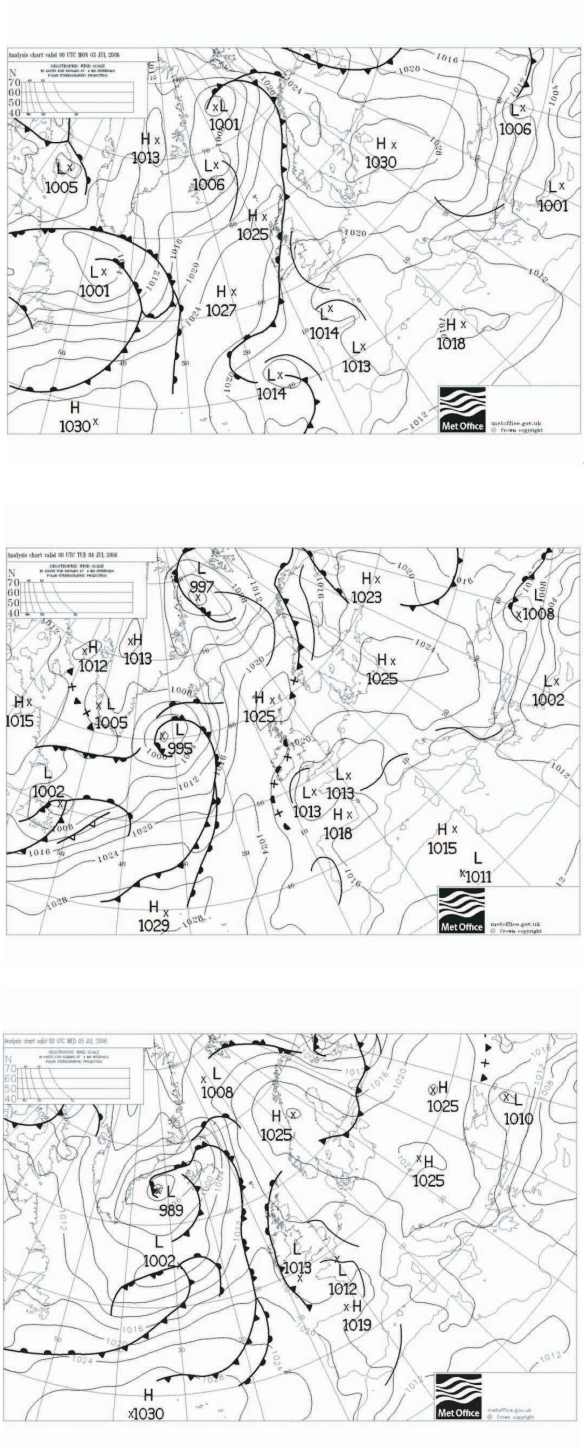

Figure 6.10: Same as Fig. 6.1, but for 3 (top), 4 (center), and 5 (bottom) July 2006.

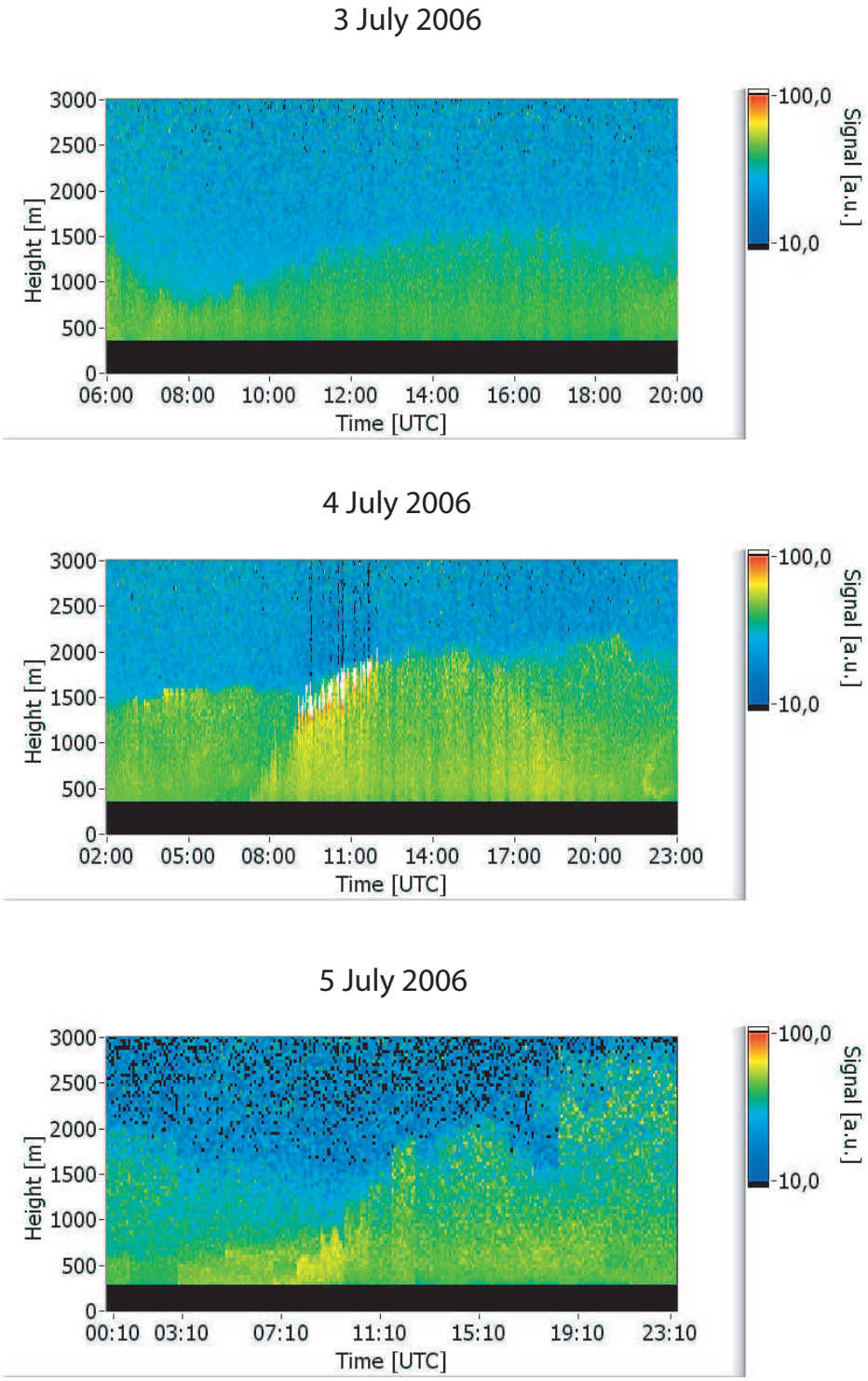

Figure 6.11: Evolution of the PBL observed with Polly on 3–5 July 2006. Range-corrected signals are shown. Continuous measurements with a resolution of 30 s were performed on 3 and 4 July 2006. For 5 July 2006, 5-minute measurements are shown, that were taken once per hour throughout the day.

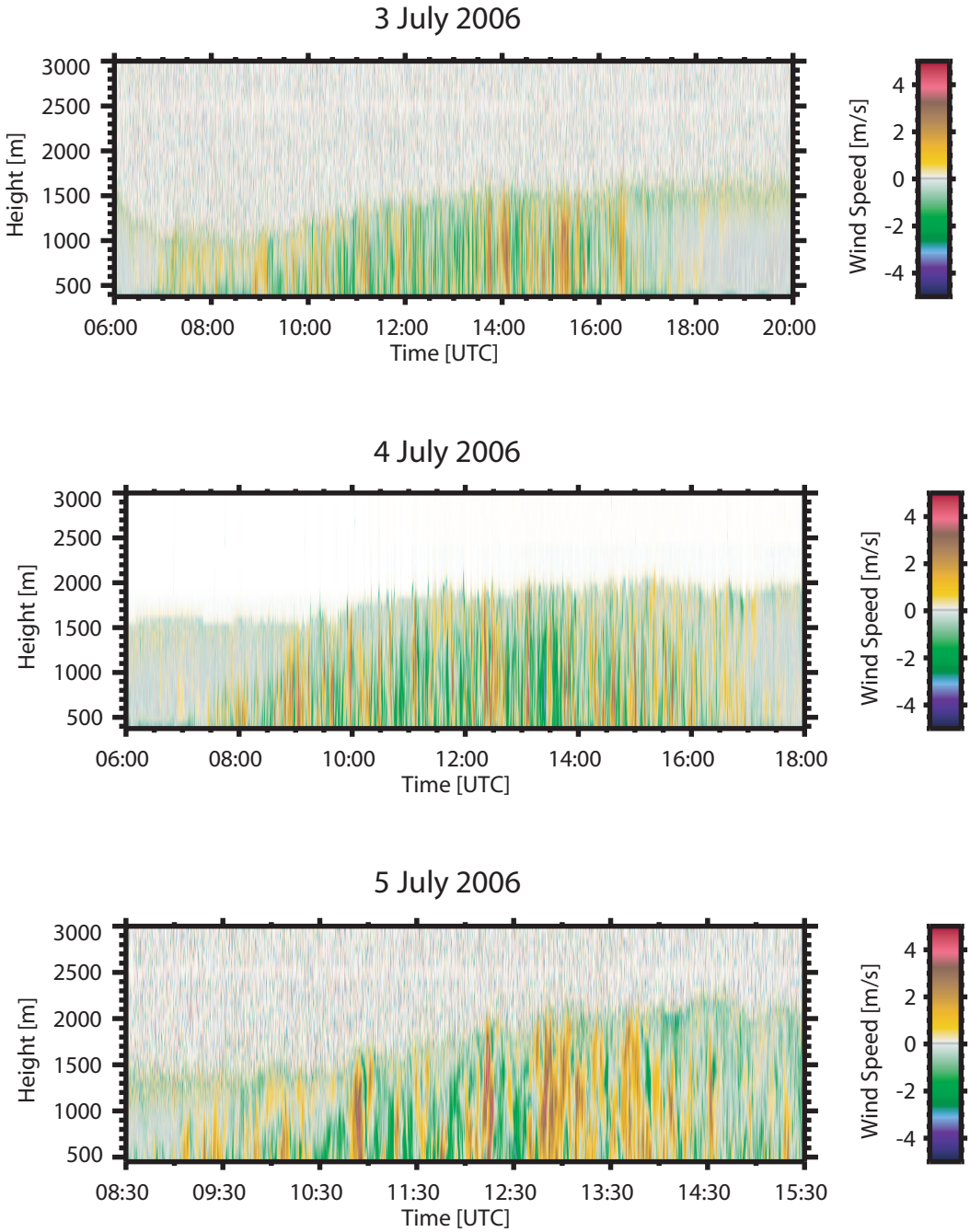

Figure 6.12: Vertical wind speed within the PBL measured with WiLi on 3–5 July 2006. The resolution is 75 m and 5 s.

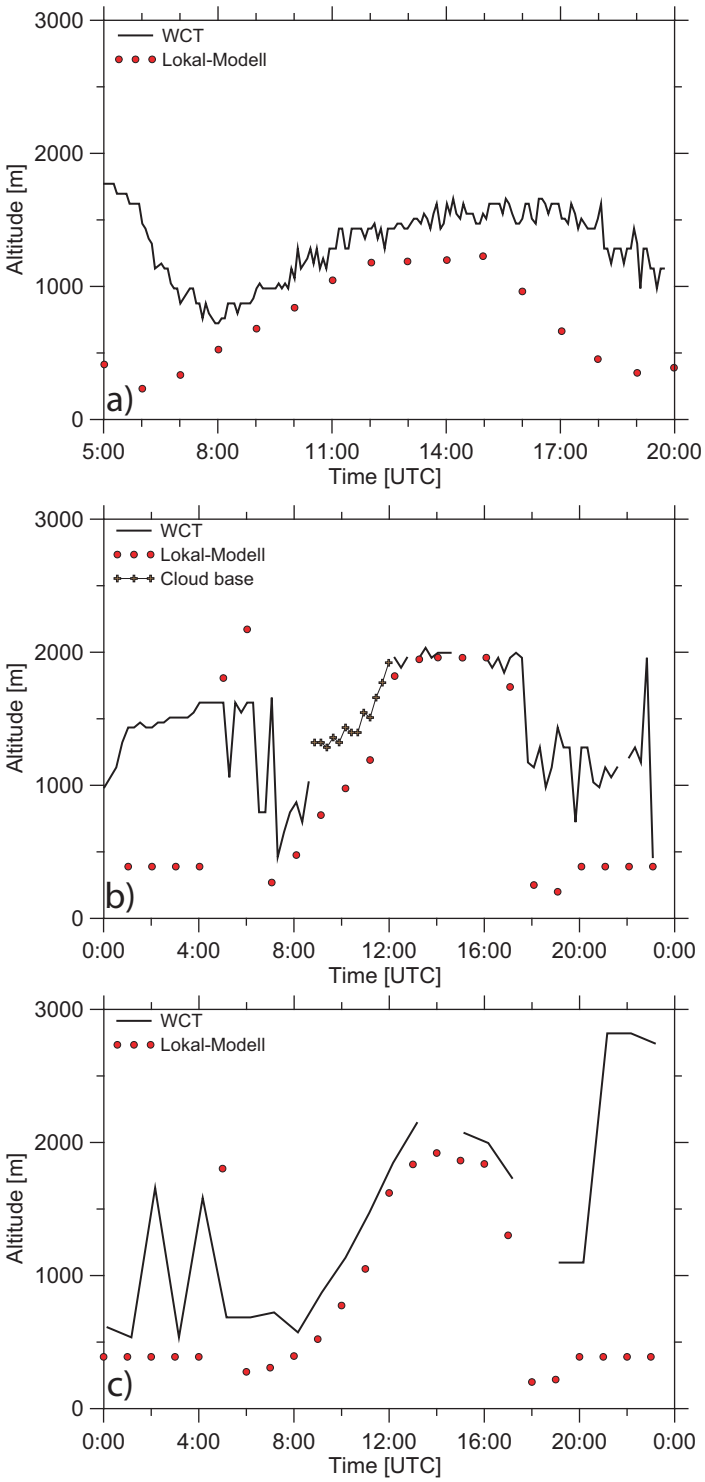

Figure 6.13: Temporal development of PBL top height observed on a) 3 July, b) 4 July, c) 5 July 2006. PBL top heights obtained with the WCT technique are compared with the respective values obtained with the LM. Crosses (center panel) indicate cloud base heights as detected with Polly.

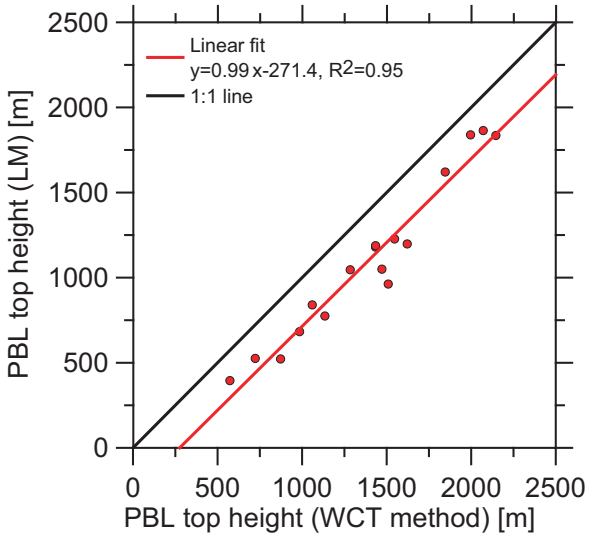

Figure 6.14: PBL top height determined with the atmospheric model LM versus the PBL top height determined with the WCT method. Data from 3 and 5 July 2007, 08:00 to 16:00 UTC are considered. The linear regression line is computed in addition. The respective equation and the quadratic correlation coefficient R^2 are given as well.

the underestimation. But it is generally known, that turbulence is underestimated in diagnostic turbulence schemes of numerical weather prediction models, especially in convective situations (Fay 1998). A good agreement between the Polly and the LM results is observed on 4 July 2006 after the clouds dissolved.

Let us finally compare the PBL growth rates observed on 3 and 5 July 2006. Both, Polly and LM, resolved the rather different growth rates, i.e., 137 m/h on 3 July and 316 m/h on 5 July according to the Polly measurements between 08:00 and 12:00 UTC. Consequently, the mean growth rate on 5 July is more than a factor of two higher than the value observed on 3 July. Almost the same meteorological conditions (temperature, humidity, radiation) were observed at the surface on these two days. The main reason for the different PBL development is the increasing influence of the low-pressure system over western Europe (see Fig. 6.10). According to Fig. 6.15, the PBL development at Leipzig was strongly suppressed by the influence of the high-pressure system over eastern Europe on 3 July. This influence weakened on 4 and 5 July. While large-scale subsidence prevailed at the 700 hPa level on 3 July, large-scale lifting dominated on 5 July.

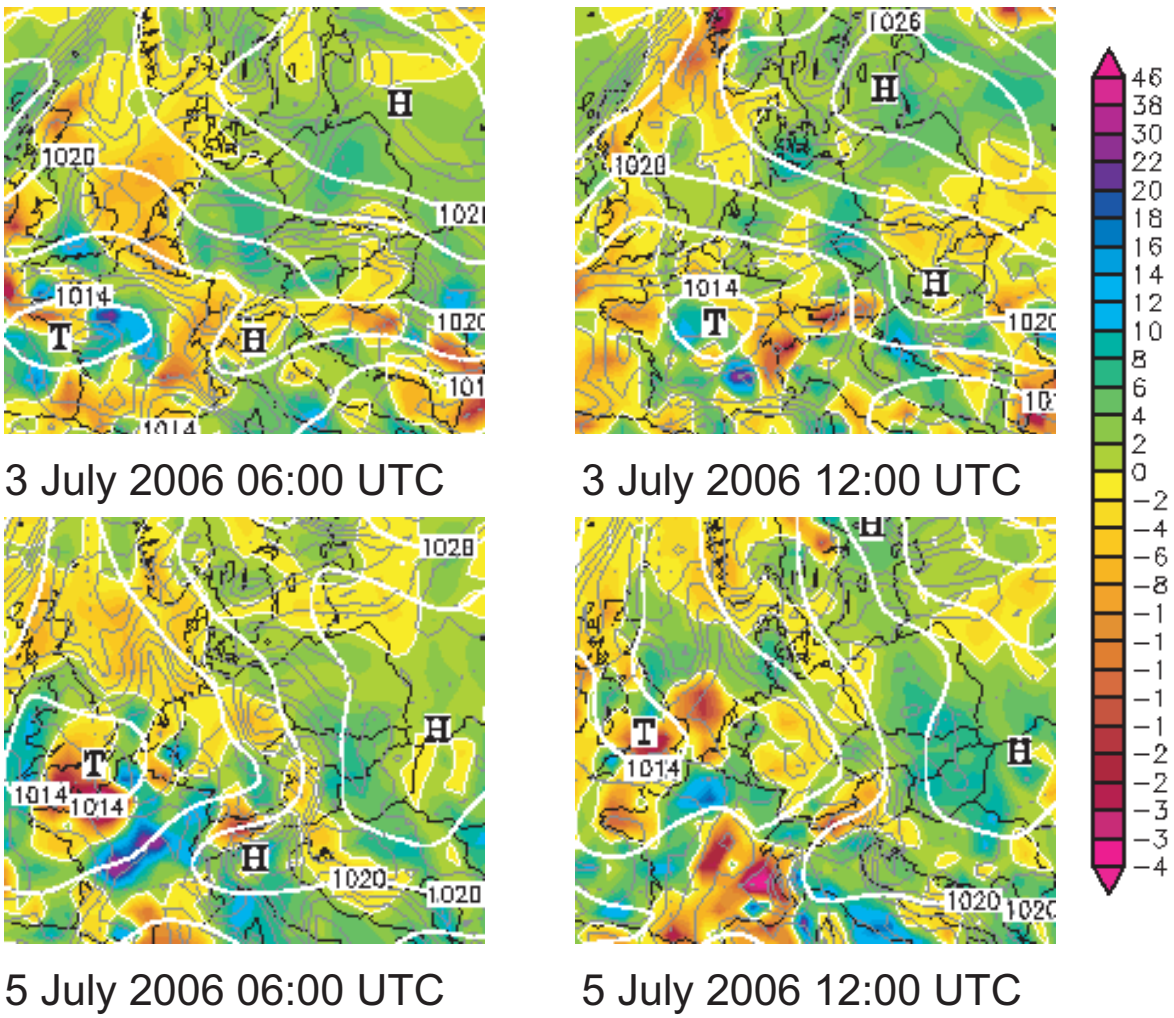

Figure 6.15: GFS analysis of 700 hPa vertical velocity, surface level pressure, and 850 hPa frontal zones provided by http://www.wetter3.de for 3 and 5 July 2006, 06:00 and 12:00 UTC. Ascend (yellow to red) and descend rates (green to blue) at the 700 hPa level are shown [hPa/h]. White lines are surface-level pressure isolines [hPa]. Grey lines are isolines of equivalent potential temperature at the 850 hPa level.

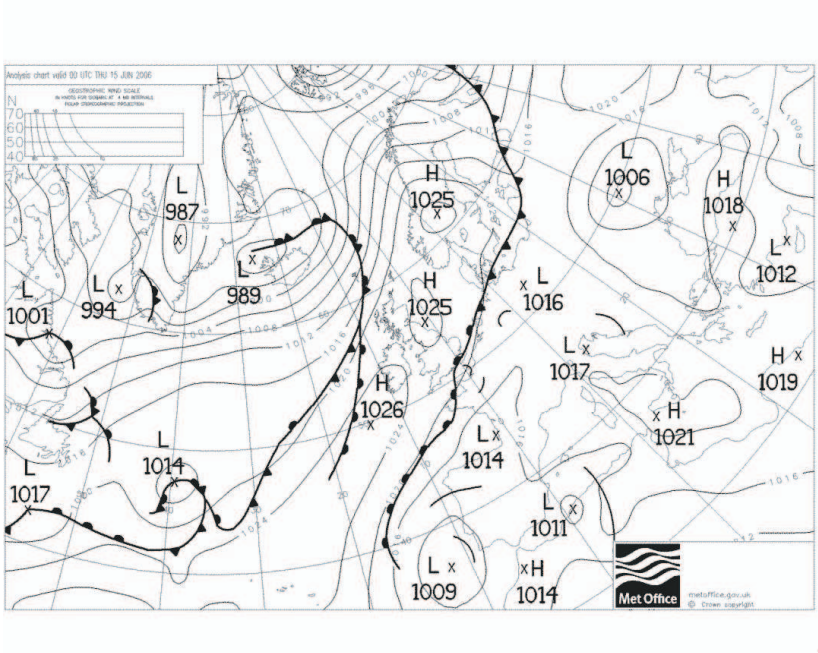

Figure 6.16: Same as Fig. 6.1, but for 15 June 2006.

6.3 15 June 2006

A low-pressure system over eastern Europe and a high-pressure system over the British Isles influenced the weather in central Europe on 15 June 2006 (Fig. 6.16). Additionally, a weak low-pressure system was present over Germany.

Fig. 6.17 shows the range-corrected signal derived from the five-minute observations once per hour. The weak signal at 13:10 and 14:10 UTC was caused by problems with the air-conditioning system of Polly on that day. The weak signal at 03:10 UTC was probably caused by fog and the correspondingly strong attenuation of laser light in the lowest heights. Clouds at several altitudes were observed throughout the day. Aerosols up to 3 km were present. Almost no evolution of the PBL is visible in Fig. 6.17.

Fig. 6.18 shows the PBL top heights obtained with the available methods and the LM. Under these complex aerosol layer conditions, the 5-min variance method fails almost completely. The fitting method provides acceptable values between 10:00–12:00 UTC only. The other methods and the LM resolve the rather low PBL top height quite well. LM provides standard values of 389 m at nighttime.

How complicated the PBL height detection is at nighttime is illustrated in Fig. 6.19. The last 5-min period of Fig. 6.17 is shown. Several aerosol layers (below 2000 m) and cloud/aerosol layers (above 2000 m) were present. The 5-min variance method

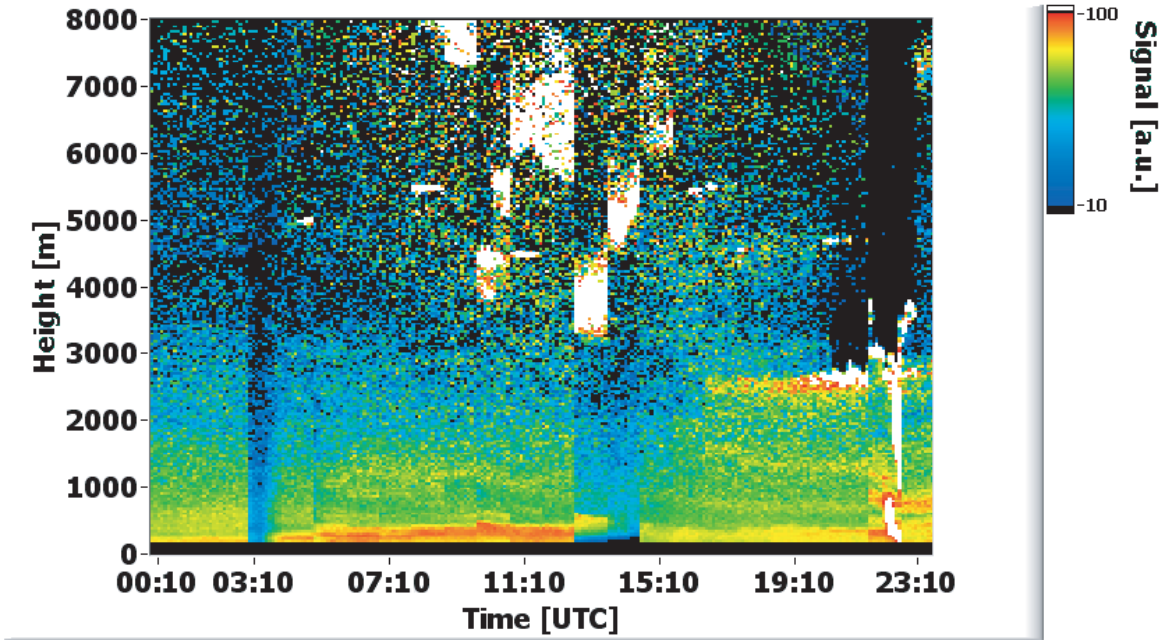

Figure 6.17: Range-corrected signal observed with Polly on 15 June 2006. The plot is based on 5-min observations once per hour.

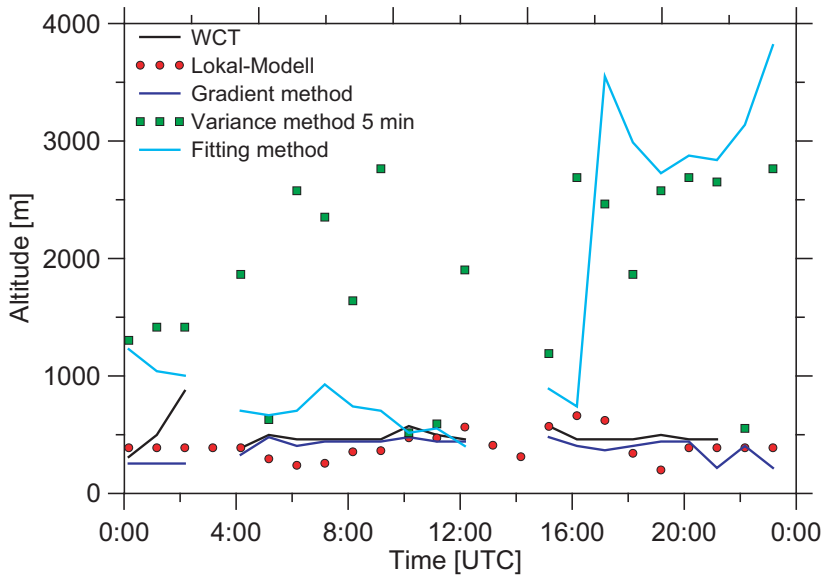

Figure 6.18: PBL top heights on 15 June 2006 derived with the methods listed in the legend. All lidar values are calculated from the 5-min long signal averages taken once every hour. No lidar values are shown for 3:10, 13:10, and 14:10 UTC because of the weak backscatter signal.

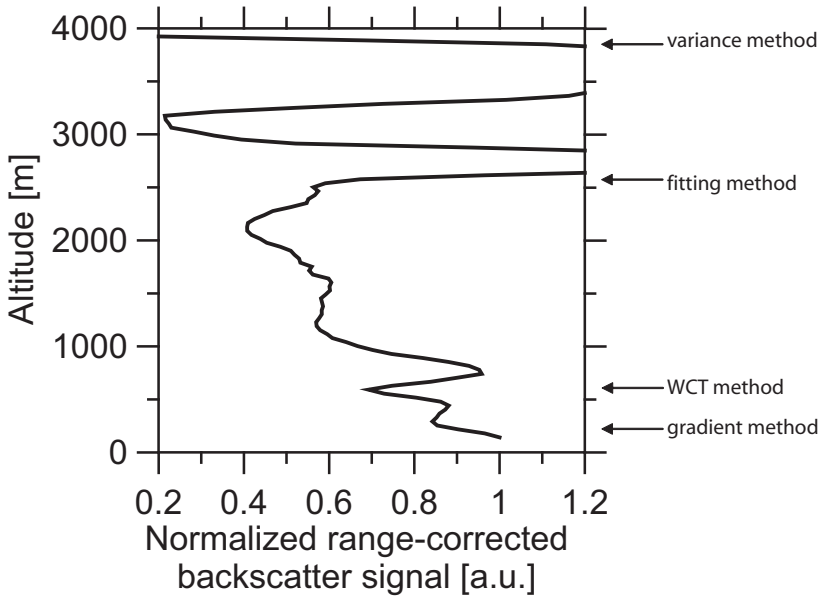

Figure 6.19: Mean range-corrected signal measured with Polly on 15 June 2006, 23:08–23:13 UTC. PBL top heights as derived by the different methods are indicated by arrows.

interprets the backscatter peak at 2763 m height as PBL top, because of the strong signal variability in this height region. The gradient method selects the first strong backscatter at about 220 m as the PBL height. The WCT algorithm finds the PBL top at about 570 m height. The fitting method should not be applied to such complex layer cases, because of the assumption of an ideal backscatter profile with only one significant step leads to rather unrealistic PBL top heights in the fitting procedure. Here the PBL top is set to 3815 m height with this method, which corresponds to the strong signal decrease within the cloud.

Finally, the reason for the rather shallow PBL on this summer day is discussed. Insolation was significantly suppressed by the clouds on this day (cf. Fig. 6.20). The surface air temperature increased from values from of about 15 °C at 05:00 UTC to 28 °C in the afternoon. Fig. 6.21 shows the profile of the virtual potential temperature measured with radiosonde at Oppin at 00:00 UTC on 15 June 2006. In addition, the profile of the gradient Richardson number [see Eq. (2.6)] is plotted. With $Ri_c = 0.38$ (cf. Sec. 5.1) the PBL top height is found at 150 m. A very large value of $Ri > 10$ was observed at 350 m indicating a very stable stratification. At this height, the profile of virtual potential temperature indicates a strong inversion layer. This strong inversion together with the occurrence of clouds prohibited the evolution of the PBL on 15 June 2006.

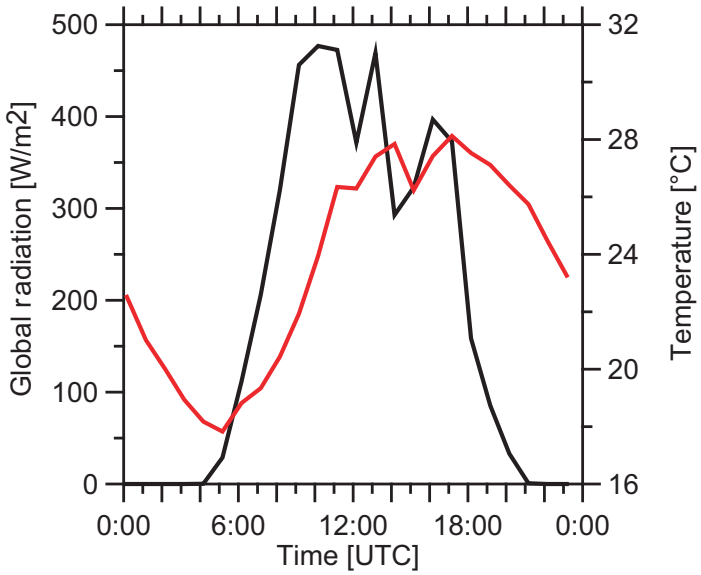

Figure 6.20: Diurnal cycle of surface temperature (red line) and global radiation (black line) observed at IfT on 15 June 2006.

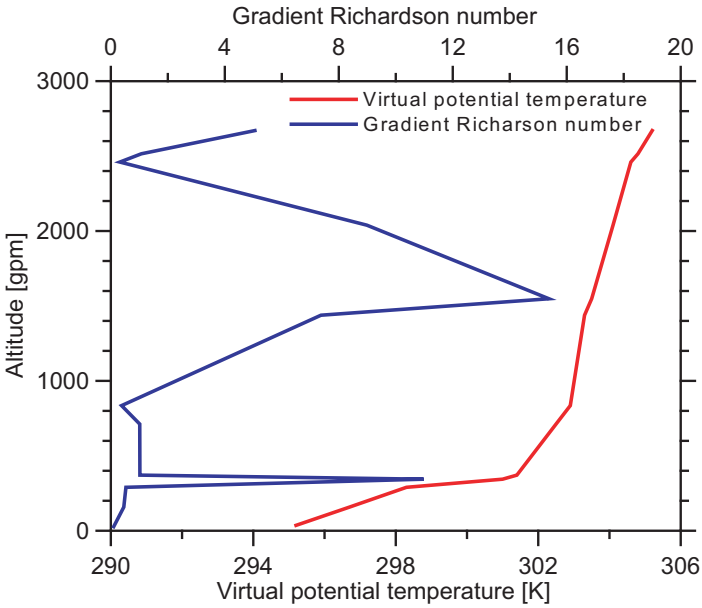

Figure 6.21: Virtual potential temperature (red line) and gradient Richardson number (blue line) versus height derived from the Oppin radiosonde on 15 June 2006 at 00:00 UTC.

Chapter 7

Statistical analysis (February 2006–January 2007)

Routine Polly measurements from February 2006 to January 2007 are statistically analyzed. The 24 five-minute observations per day are used in this study. During 7650 out of the total 8760 five-minute periods lidar measurements were possible. Data coverage is thus 87%.

7.1 PBL top height

For 3831 out of the 7650 five-minute observation periods the PBL top height could be determined with the automated WCT method. An overview of the monthly coverage regarding possible measurements and PBL top height determination is given in Fig. 7.1. Low clouds, the lack of a significant gradient in the backscatter profile, or precipitation prohibited the PBL depth determination in about 50% of the measurements. It should be mentioned that the WCT algorithm determines mostly the top of the residual layer at nighttime. Only in a few cases, typically in situations with strong winds, the nocturnal PBL could be determined. For that reason, we restricted the statistical analysis of PBL top height to measurements which were taken four hours after sunrise to one hour before sunset. Thus, the following figures cover the daytime PBL only.

Fig. 7.2a shows all individual daytime PBL top heights and the corresponding 7-day moving average. The annual cycle with low PBL top heights in winter and high values of the PBL top in summer is clearly visible. The influence of the synoptic conditions is indicated by the high variability in the 7-day running mean. The annual cycle is

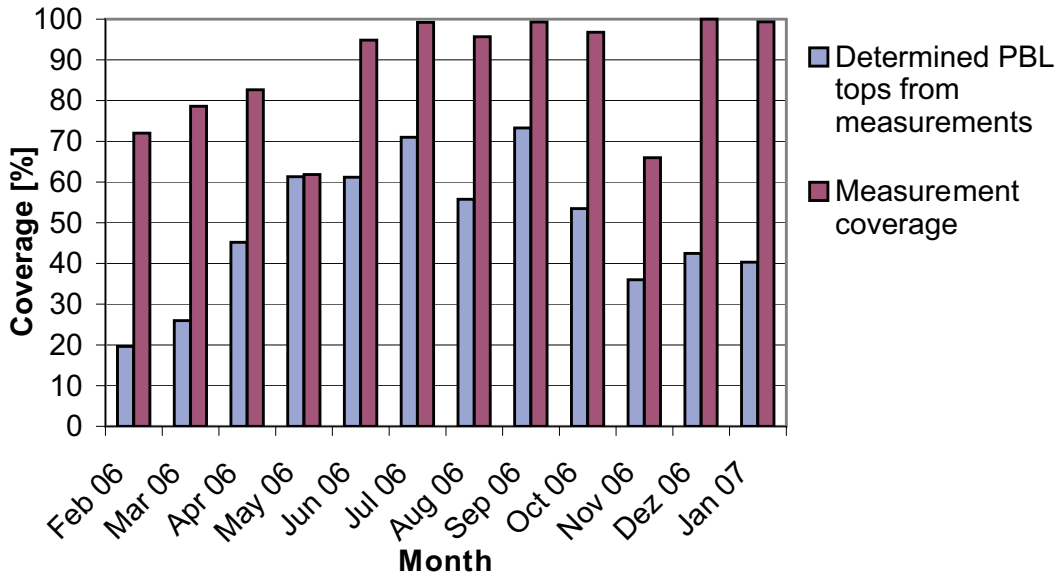

Figure 7.1: Number of measurements performed with Polly relative to the number of theoretically possible measurements in the time period from February 2006–January 2007 (red) and number of determined PBL depths relative to the number of taken measurements (blue).

even more pronounced when values of the daily maximum PBL depth are considered only (cf. Fig. 7.2b).

In Fig. 7.3a and b, the monthly means of the individual daytime PBL depth and of the daily maximum PBL top height are shown, respectively. Except for July 2006, nearly constant values are found in Fig. 7.3a in the period from April to September. Significant lower values are observed from October to March. Weather conditions, like the relatively cold August 2006 and the mild Winter 2006/2007, are clearly reflected in the observed mean and mean maximum PBL depths. Remarkable is the mean daily maximum PBL depth of 2235 m in July 2006.

Fig. 7.4a and b present histograms of the PBL top heights and the daily maximum PBL depths for the different seasons, respectively. As can be seen in Fig. 7.4a, a very narrow distribution is observed in winter. More than 90% of all values are below 1000 m in this season. The shape of the distributions in spring and fall is quite similar. A clear peak is observed for PBL depths between 750 and 1000 m. More than 90% of all values are below 2000 m in both distributions. In summer, a very broad distribution is observed without a clear peak. 80% of the values are between 500 and 2000 m.

As can be seen in Fig. 7.4b, winter daily maximum PBL depths often do not exceed

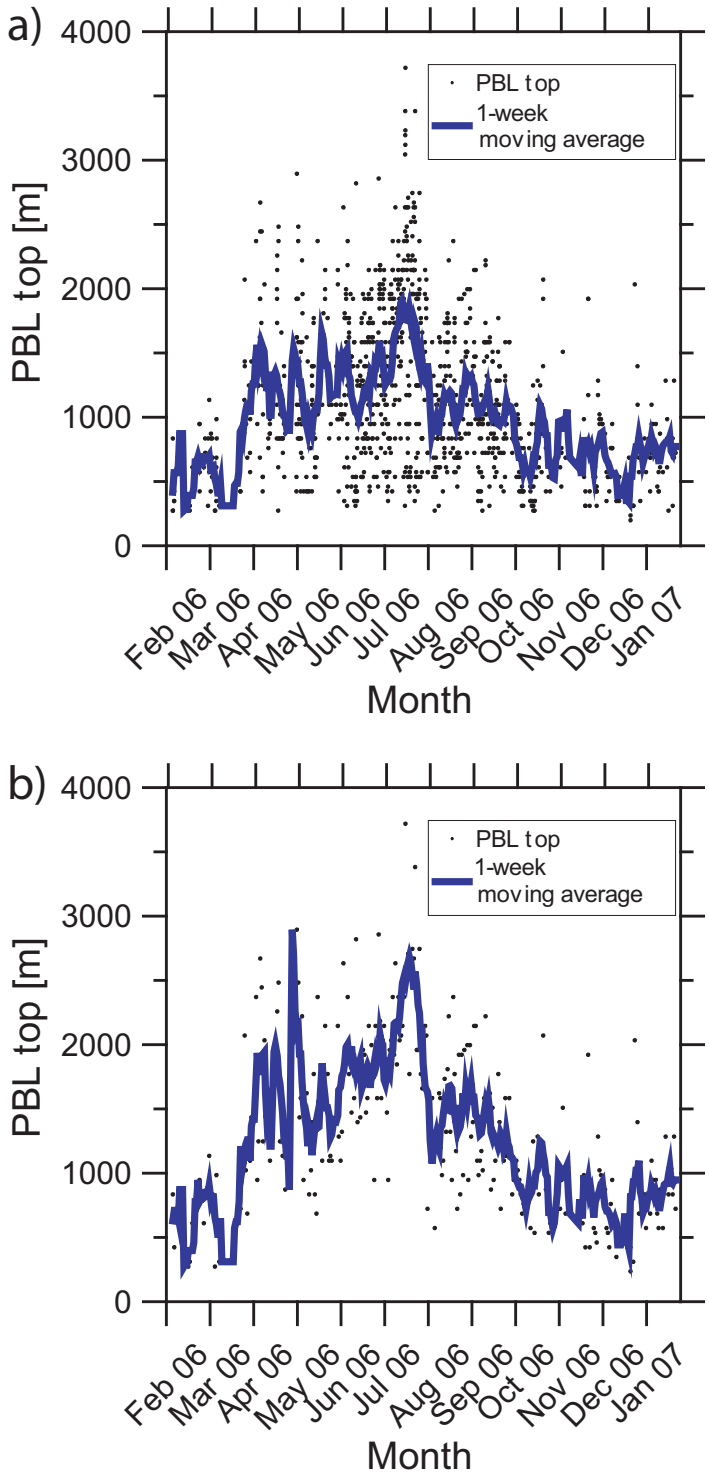

Figure 7.2: a) Daytime PBL top heights determined with Polly. Individual measurements (dots) and the 7-day running mean (solid line) from February 2006 to January 2007 are shown. b) Same as a), but for daily maximum PBL top height.

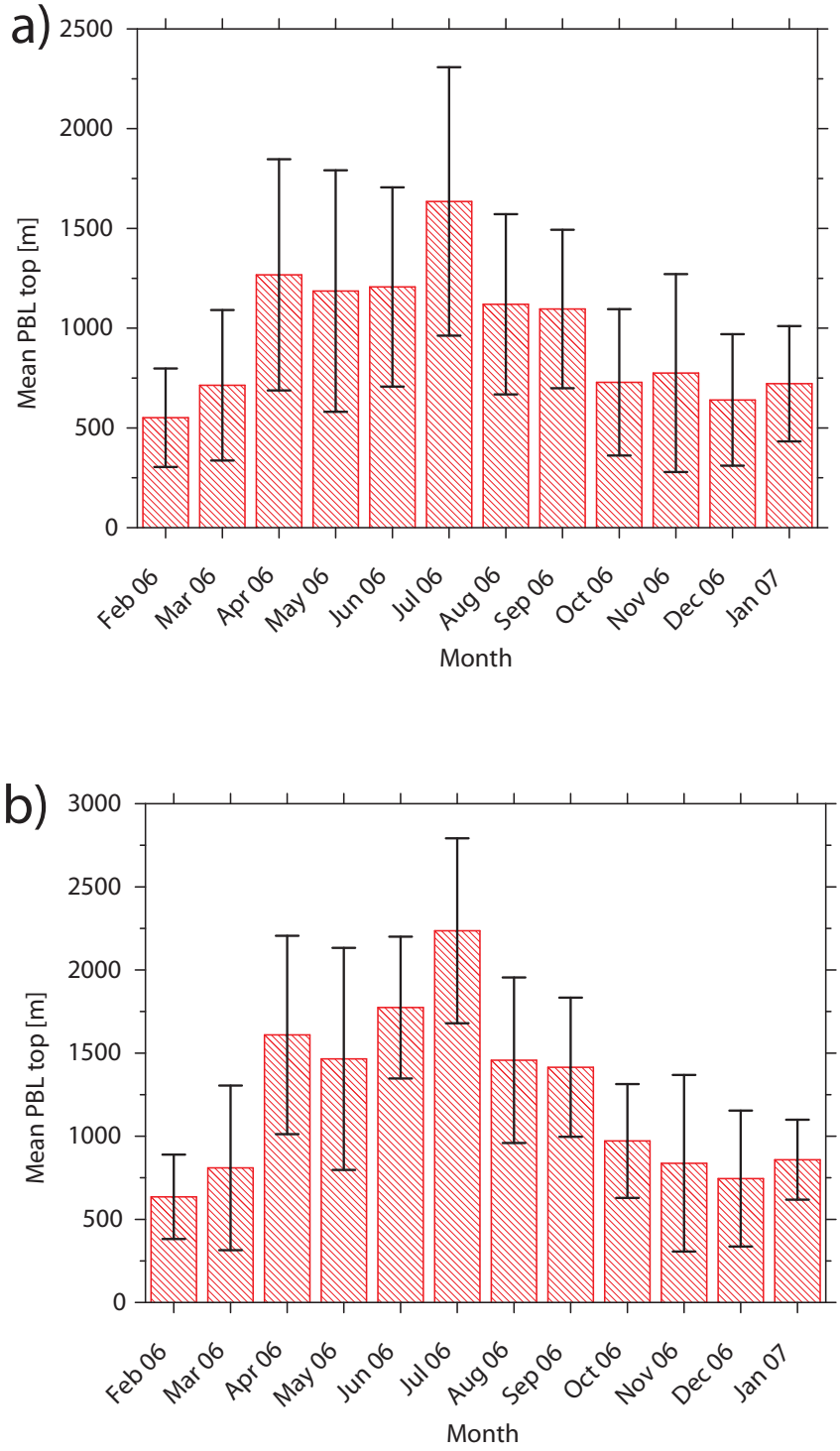

Figure 7.3: a) Monthly mean daytime PBL top heights determined with the WCT method from Polly measurements from February 2006 to January 2007. b) Same as a), but for daily maximum PBL top height.

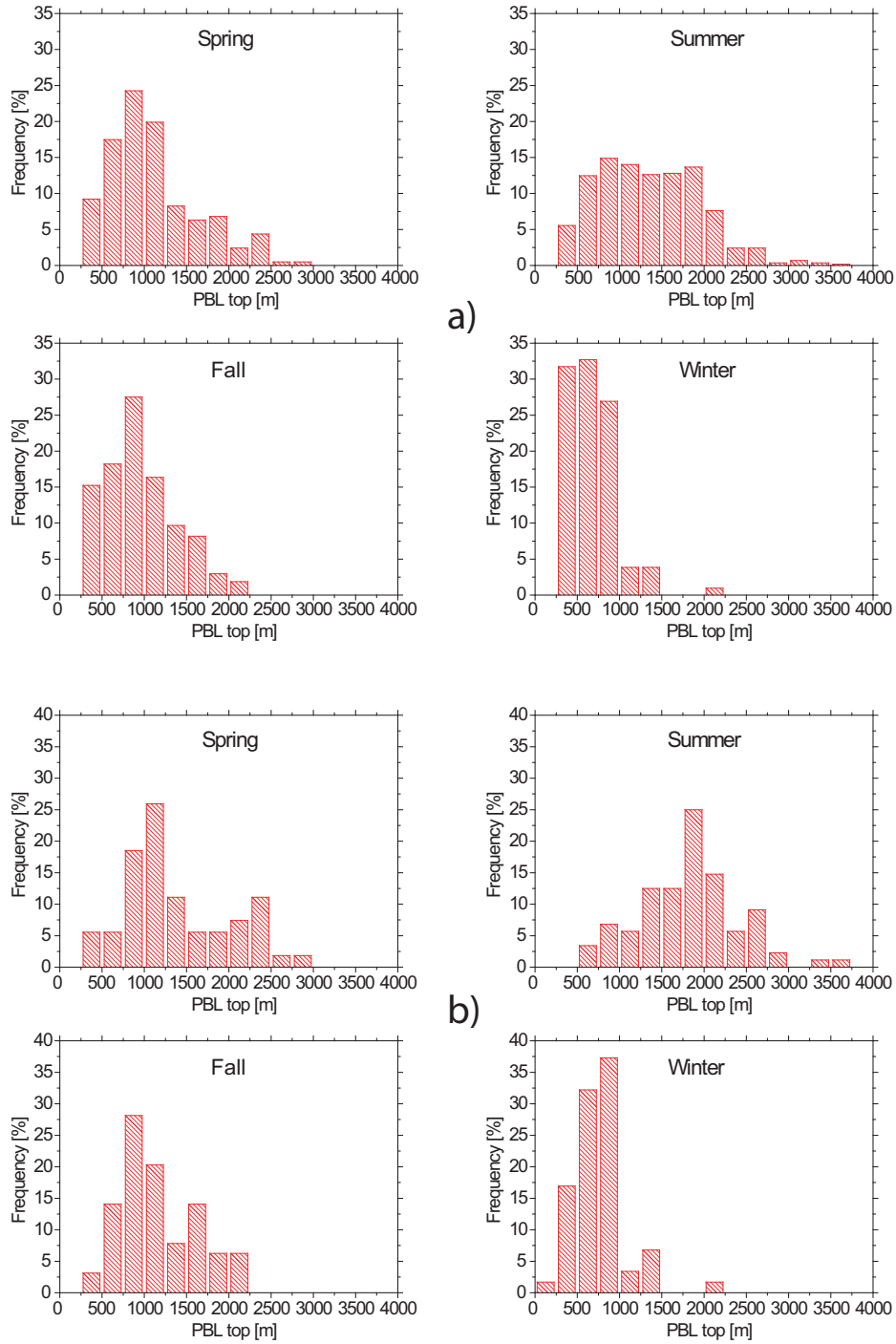

Figure 7.4: Frequency distributions of a) daytime PBL top, b) daily maximum PBL depth.

Table 7.1: Comparison of PBL top height observations (Polly) with EARLINET lidar observations at Leipzig presented by Mattis et al. (2004). EARLINET observations cover the period from May 2000 to March 2003.

Season	Mean PBL depth (shortly after sunset)	Mean value of the daily maximum PBL depth	Mean RL depth (Mattis et al., 2004)
Spring	1282±697 m	1385±637 m	1850 m
Summer	1515±629 m	1836±589 m	2450 m
Fall	994±452 m	1165±456 m	1300 m
Winter	782±375 m	798±354 m	950 m

1000 m (>80%). In summer, a very broad distribution is observed with a maximum between 1750 and 2000 m. In 35% of all cases, a growth of the PBL to a depth of more than 2000 m was observed. Over 50% of the observed maxima are between 750 and 1500 m in spring. In fall, most daily maximum PBL depths are between 500 and 1250 m (>60%).

In Tab. 7.1 the PBL statistic is compared with the residual-layer statistic presented by Mattis et al. (2004). The latter measurements were performed within the EARLINET (European Aerosol Research Lidar Network) project at the IfT from May 2000 to March 2003. These observations were usually done shortly after sunset and the detected residual-layer height was interpreted as the maximum PBL top height of that day.

The comparison of the Polly measurements (Tab. 7.1, columns 2 and 3) reveals that the PBL measured shortly after sunset is generally lower than the observed daily maximum. This can be explained with an often observed descent of the RL top height which starts already before sunset as, e.g., Fig. 6.3a and Fig. 6.5a show. The comparison also reveals that both, the mean maximum PBL depths and the values observed shortly after sunset, are generally lower than the ones observed by Mattis et al. (2004). The fact that EARLINET measurements are usually only performed in the absence of low-level clouds but Polly measures routinely could be a reason for the observed difference. But we also have to keep in mind that measurements in 2006/2007 (one year) are compared with data from a three-year period (2000–2003). Different meteorological conditions, e.g., a cold May and August with low PBL top heights in summer 2006 may have also caused the differences.

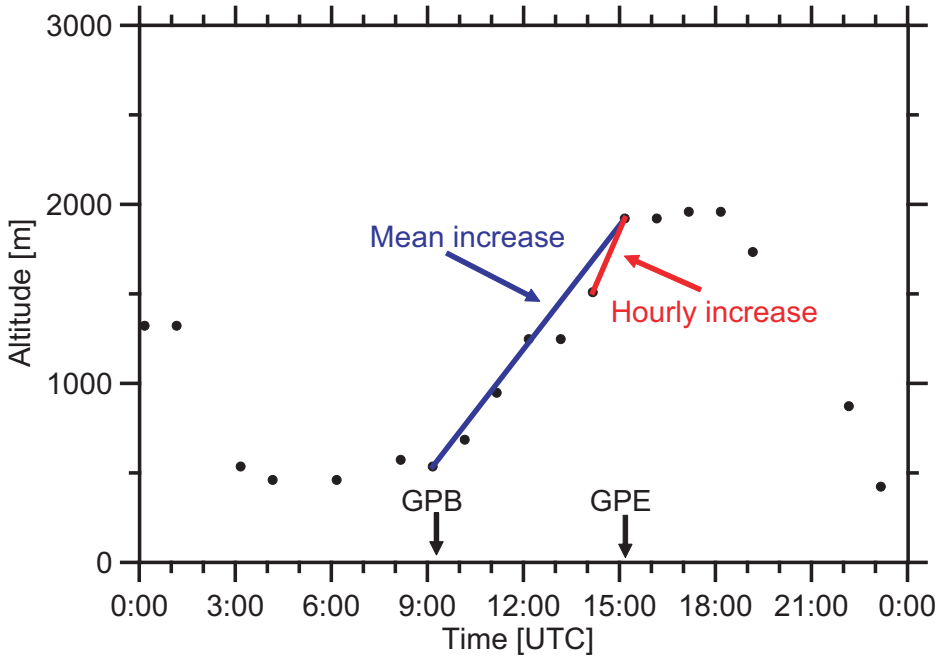

Figure 7.5: Hourly and mean growth rate of the PBL top height on 28 July 2007. Dots indicate individual PBL top heights identified with Polly. GPB: denotes that time at which the PBL starts to grow significantly. GPE: denotes that time at which the PBL growth is almost completed.

7.2 PBL diurnal cycle and growth rate

65 days in 2006/2007 could be used to study the growth of the PBL depth in the morning and early afternoon hours. In the following, we denote the increase of the PBL top height within one hour as hourly growth rate. Similarly, the mean growth rate describes the increase of the PBL top from the nocturnal value (about 4 hours after sunrise) to the maximum value (at about 13:00–14:00 UTC). The 65 useful days present days without fog and precipitation. No significant air-mass change, e.g., caused by frontal passages occurred on these days. Finally, at these days the minimum PBL top height could be clearly identified with Polly. Therefore, most of the analyzed cases are in the summer period. Fig. 7.5 illustrates the determination of the hourly and mean PBL growth rates. In practice, we define the main growth period with significant PBL height increase as the period from the time when significant growing of the PBL starts (GPB for growth period begin) to the time at which the PBL top height is at least 90% of the maximum PBL depth observed on this day (GPE for growth period end). The results of this study (based on the 65 days) are shown in Fig. 7.6a and b for the hourly and the mean growth rates, respectively. Because of the strong annual cycle

of incoming radiation, higher values of the hourly and the mean PBL growth rate are observed in the summer period from April to September. The maximum hourly growth rate is 937 m/h, observed on 4 May 2006. The maximum mean growth rate of 512 m/h was observed on 13 July 2006.
Histograms of observed hourly and mean growth rates are shown in Fig. 7.7a and b, respectively. Most hourly growth rates are below 300 m/h (>75%). Hourly growth rates of more than 600 m/h are rare (<3%). Typical values of the mean growth rate are between 100 and 300 m/h (>50%). Values of more than 500 m/h are observed in less than 2% of all analyzed cases. The observed values of GPE (time at which the main growth of PBL stops) and the corresponding histogram are shown in Fig. 7.8a and b, respectively. In more than 80% out of all analyzed cases the growth phase ends between 11:00 and 14:00 UTC. The time difference between UTC and the local solar time in Leipzig (51.35 N, 12.43 E) is approximately +1 hour (exactly +50 min). Thus, the main PBL growth is usually completed between 12:00 and 15:00 local solar time. A clear annual variation is not observed.

7.3 Comparison with LM-derived PBL top heights

PBL top heights calculated from the LM temperature and wind fields are available for each full hour (00:00, 01:00...23:00 UTC). The PBL top heights are measured with Polly from minute 8–13 of each hour.
At nighttime the LM provides standard values only, and Polly often detects the RL after sunrise and in the late afternoon. Therefore, only values between 10 and 14 UTC are used in Fig. 7.9a, which shows the comparison of the hourly PBL top heights. Fig. 7.9b presents a comparison of the corresponding daily maximum PBL depth from Polly and LM. Disregarding the large scatter in the data points, a systematic underestimation of the daytime PBL depth by the LM is visible in both comparisons (on average about 20%). Strong deviations (LM PBL depth >2000 m, lidar PBL depth <1000 m) can occur in cases with clouds (not predicted by the LM) or during cloud-free conditions (LM PBL depth <1000 m, lidar PBL depth >2000 m).
Another possible reason for strong deviations is shown in Fig. 7.10. A phase shift in the PBL evolution of about 3 hours between the Polly and the LM time series was observed on 8 March 2006. The reason possibly was an air-mass change that occurred earlier than predicted by the LM. But also small phase shifts can lead to large differences as found on 5 July 2006, 11:00 UTC (Fig. 6.13c).
The comparison of the daily mean growth rates obtained from Polly and LM data for

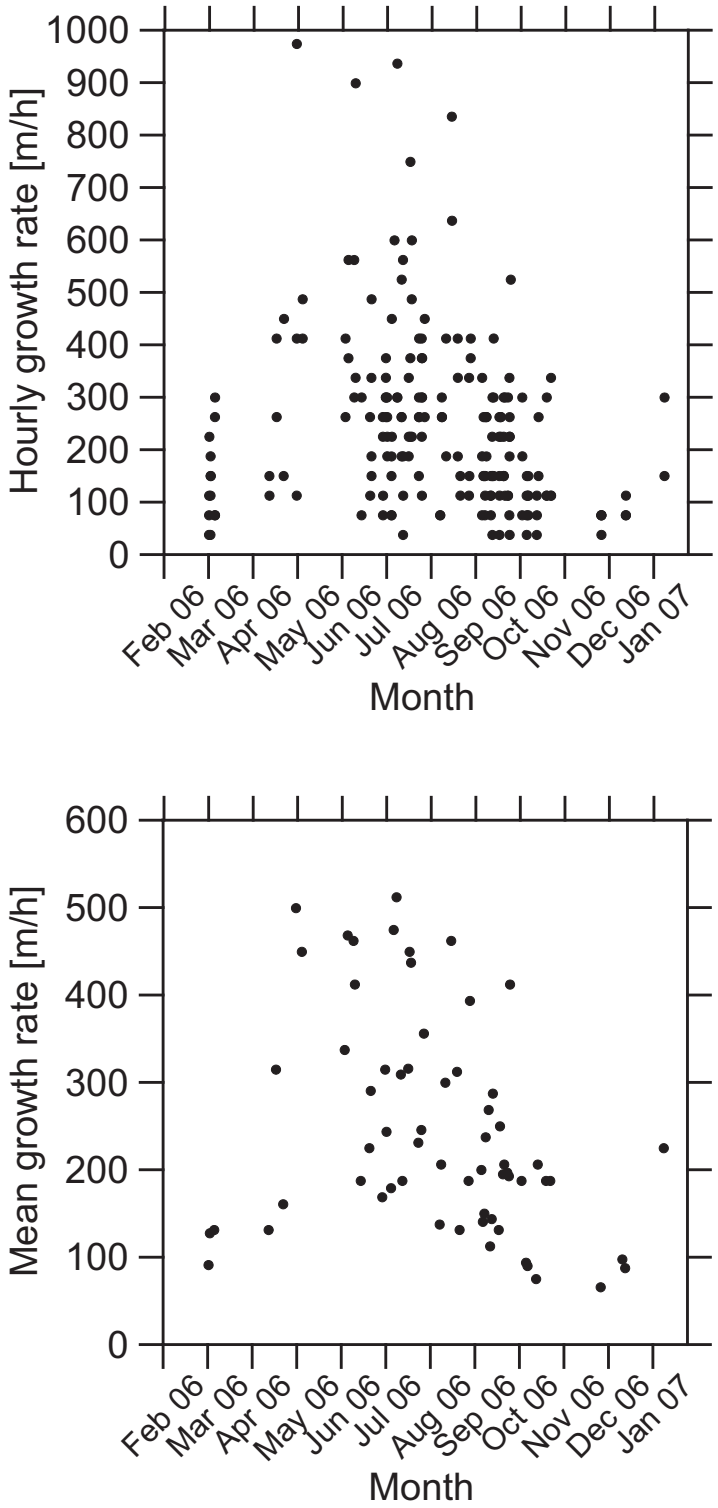

Figure 7.6: Daily a) hourly and b) mean PBL growth rate as observed from February 2006 to January 2007.

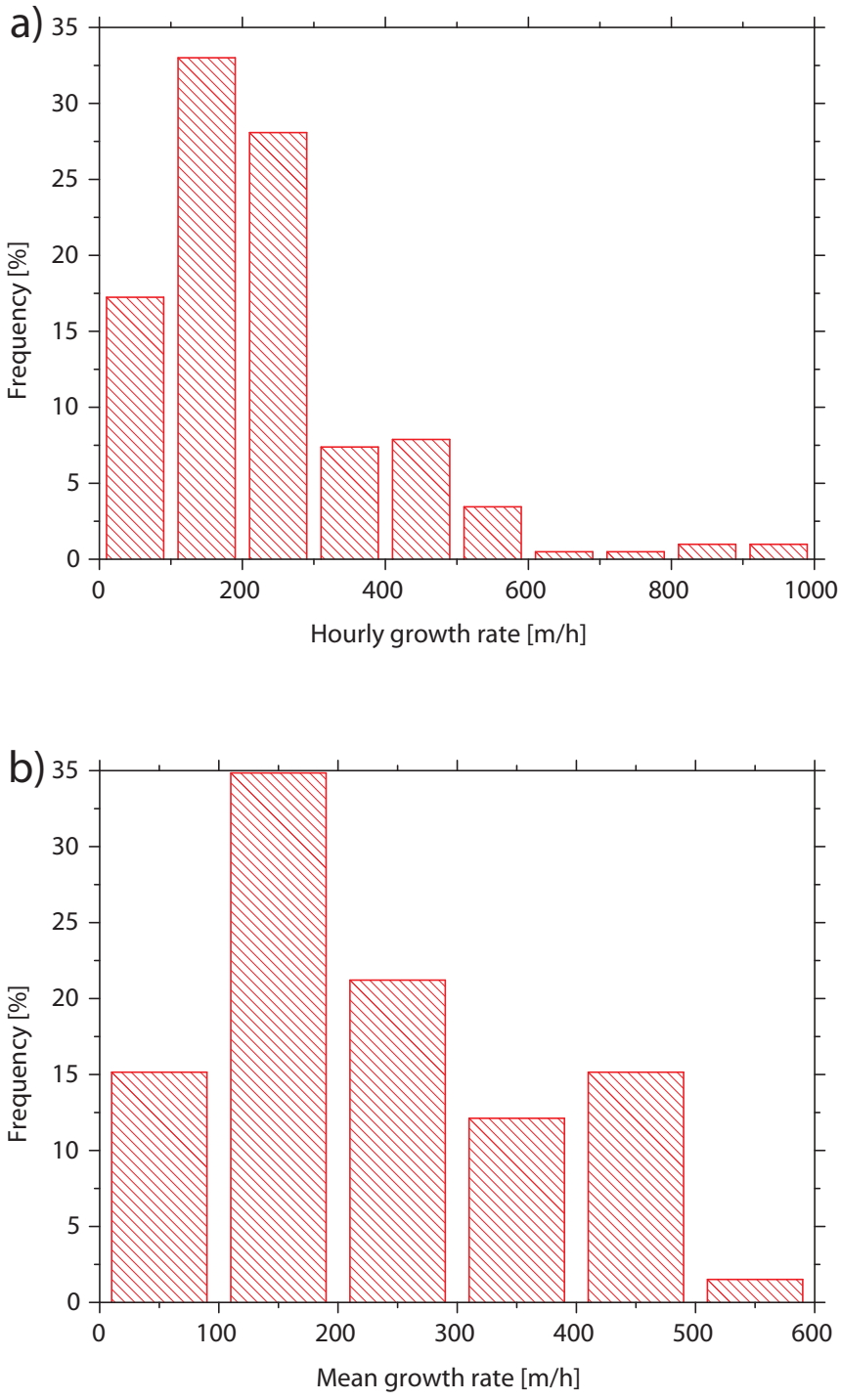

Figure 7.7: Frequency distribution of observed a) hourly and b) mean PBL growth rate.

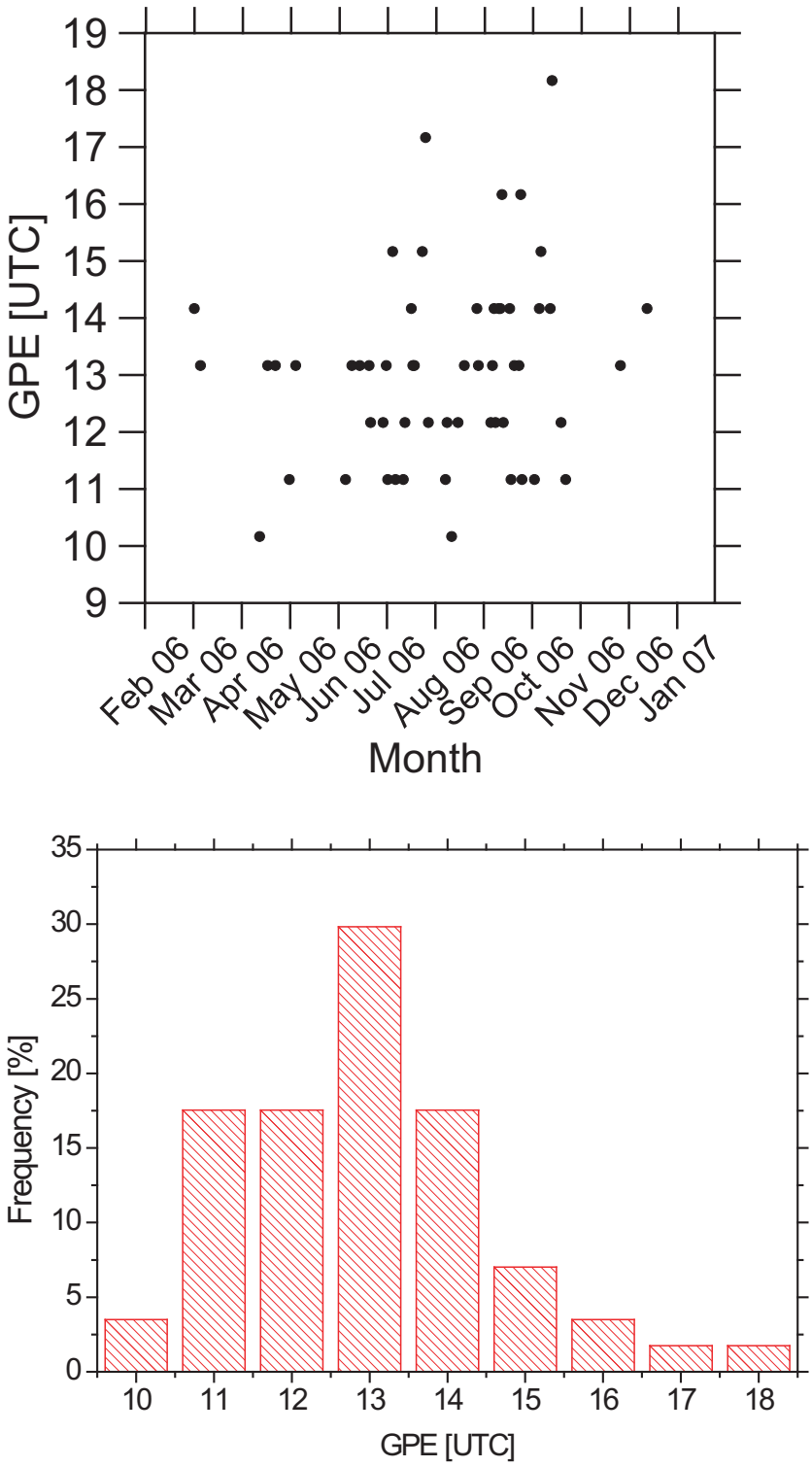

Figure 7.8: a) Time series of GPE (time at which the main growth phase of the daily PBL evolution is completed) and b) corresponding frequency distribution.

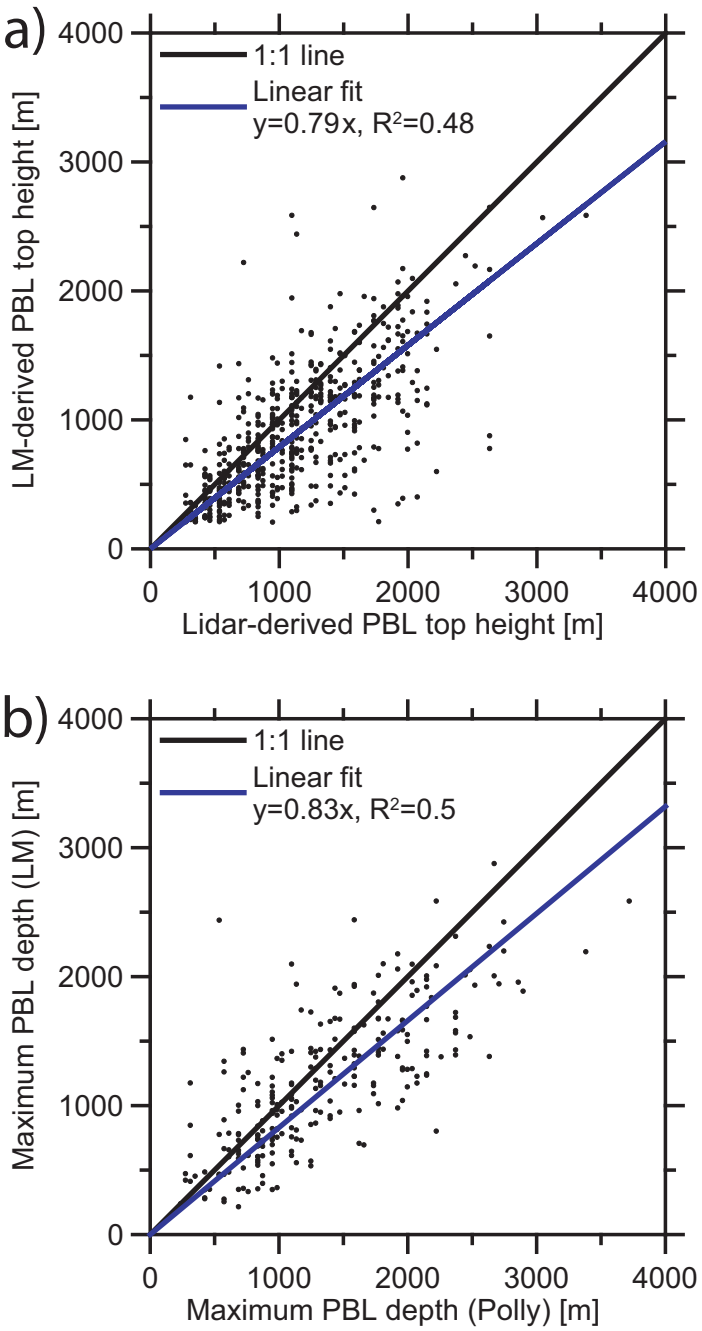

Figure 7.9: Comparison of PBL top heights as derived from lidar observations and estimated from LM model data, a) between 10 and 14 UTC, b) for the daily maximum. Linear regression lines are computed in addition. The respective equations and the quadratic correlation coefficient R^2 are given as well.

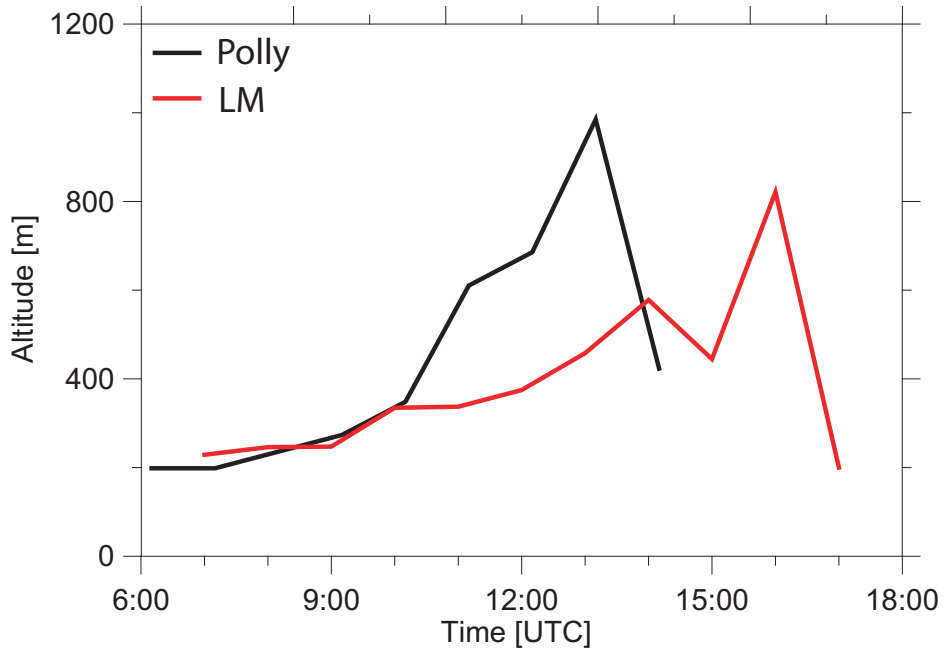

Figure 7.10: PBL top heights derived from Polly data and LM data on 8 March 2006.

the 65 chosen days (see Sec. 7.2) is presented in Fig. 7.11. A reasonable agreement is observed up to values of about 300 m/h. The corresponding linear regression line for values below 300 m/h is also shown. According to this fit, an underestimation of the mean PBL growth rate from the LM of about 25% is found, which is in agreement with the investigations made above. Observed mean growth rates of more than 300 m/h are often not found in the PBL evolution predicted by the LM. In these strong convective situations, observed mean growth rates can be a factor of 3 larger than computed.
The difference in GPE (time at which the mean PBL evolution is completed) derived from Polly and LM data is shown in Fig. 7.12. A good agreement is found. Shifts by ± 1 hour are partly caused by the resolution of 1 hour in the PBL observation and LM computation. In about 25% of all analyzed cases deviations of 2 hours and more are found.

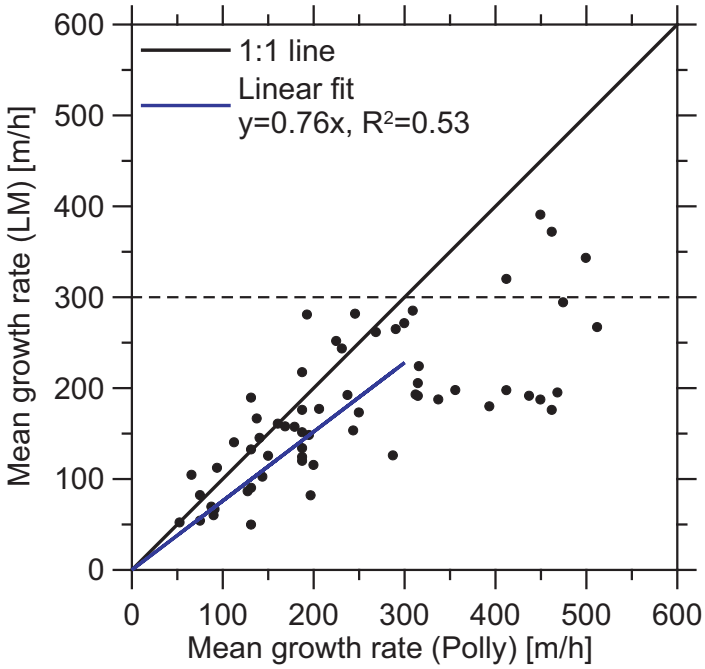

Figure 7.11: Comparison of mean growth rate of PBL depth as derived from lidar observations and estimated from LM model data.

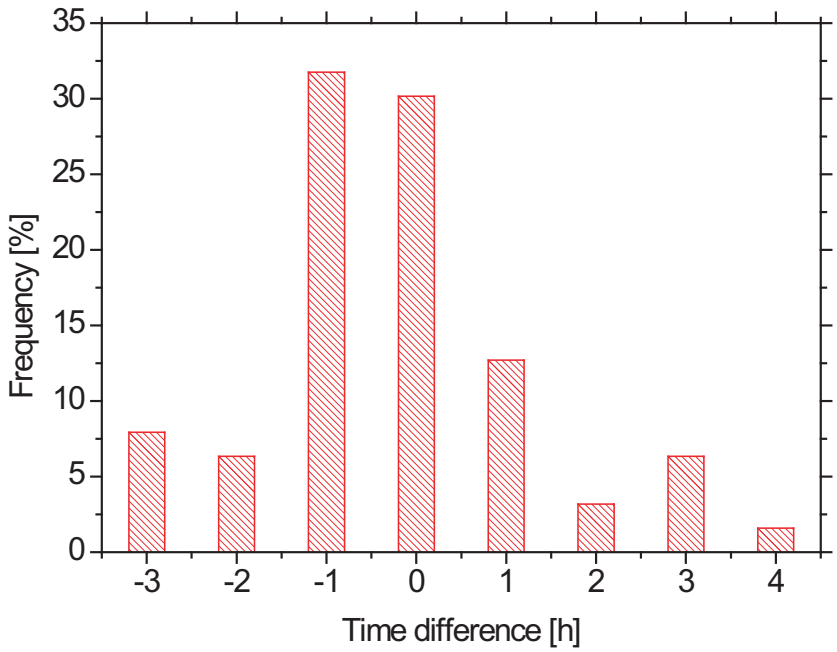

Figure 7.12: Difference $\Delta t = \mathrm{GPE}_{\mathrm{Polly}} - \mathrm{GPE}_{\mathrm{LM}}$. GPE is the time at which the main evolution of the PBL is completed.

Chapter 8

Summary

This diploma thesis showed that automated daytime PBL top height determination from continuous lidar measurements is possible with high temporal and spatial resolution and acceptable accuracy. An automated algorithm was developed which is based on the modified WCT method. The modifications include the normalization of the range-corrected signal, the introduction of a threshold, and a height-dependent dilation. A cloud-base detection method was developed and successfully tested. This screening technique allows us to remove cloud signals from the backscatter data set. This algorithm and the other lidar-based PBL depth determination methods (gradient, variance and fitting techniques) were intensively tested. Several observational case studies taken on 11–13 September 2006, 3–5 July 2006, and 15 June 2006 were discussed. The measured PBL top heights were compared with the ones that were calculated with the gradient Richardson scheme from LM temperature and wind fields to check the potential of the LM to provide PBL top heights. The LM data was provided by the German Meteorological Service (DWD). Radiosonde launches and vertical wind observations with wind lidar WiLi were used to obtain a detailed set of information on the convective state of the PBL. Especially the analysis of the vertical-wind speeds from WiLi observations allowed the determination of the period of convective mixing characterized by strong up- and downdrafts.

During the periods with pronounced convective activity all presented lidar methods were able to detect the PBL top height. Good agreement between the lidar-derived PBL top heights and the ones indicated by the radiosondes (profiles of the virtual potential temperature, water-vapor-to-dry-air mixing ratio, and the buoyancy term of the turbulence-kinetic-energy budget equation) were found. The detection of a very shallow PBL below 250 m is impossible because of the incomplete laser-beam receiver-field-of-view overlap. Consequently, in the early morning, in the late afternoon, and

during nighttime the presented lidar methods detect the top of the RL and interpret this as PBL top height. Under complex atmospheric conditions, e.g., with multiple aerosol layers or weak backscatter gradients, it was shown that the gradient, the variance and the fitting methods can have large errors. However, the introduction of the height-dependent dilation in the WCT method was found to be an important improvement that led to an accurate detection of the midpoint of the transition zone in most cases. In summary, one can conclude that the modified WCT method works best to determine the PBL top height. The comparison of the lidar and LM-derived PBL depths revealed partly good agreement (11–13 September case) and partly a systematic underestimation (3–5 July case) of the PBL top height by the LM.
Finally, the one-year Polly data set measured from February 2006 to January 2007 was statistically analyzed. The modified WCT method was used here. In 50% of all measurements a PBL top height could be determined (about 3900 values). Precipitation, low-level clouds, or the lack of a significant gradient in the backscatter profile often prohibited the determination of the PBL top height. The most trustworthy PBL depths from four hours after sunrise to one hour before sunset were considered in the statistical analysis only. Time series and frequency distributions of the daytime PBL depth and the daily maximum PBL top height show a clear annual cycle with shallow PBL in wintertime and deep PBL in the period from April to September. The synoptic influence is also clearly seen in the high variability of individual and maximum PBL top heights. Mean maximum PBL depths of about 1400 m in spring, 1800 m in summer, 1200 m in fall, and 800 m in winter were observed. These values are systematically lower than values of the RL top height (measured shortly after sunset) presented by Mattis et al. (2004) for the 2000–2003 time period. A statistical analysis of the growth behavior of the PBL over a full year was presented here for the first time. 65 days were chosen for which a clear diurnal cycle could be observed. Typical values of the hourly and mean growth rates range from 100–300 m/h. But also hourly increases of more than 900 m/h and mean increases of more than 500 m/h were observed. It was found that the growth of the PBL is usually completed between 12 and 15 local solar time. Although a large scatter in the comparison of the lidar and the LM PBL top height was found, a systematic underestimation of, on average, 20% of the PBL depth by the LM is also confirmed by the one-year data set. Reasons for the large scatter are phase shifts between observed and predicted PBL evolutions, wrong computed cloud cover, and underestimation of turbulence by the model.

Appendix A

List of Abbreviations

DWD	German Meteorological Service (Deutscher Wetterdienst)
EARLINET	European Aerosol Research Lidar Network
GFS	Global Forecast System
GPB	Growing phase begin
GPE	Growing phase end
IfT	Leibniz Institute for Tropospheric Research
LM	Lokal-Modell
Nd:YAG	Neodymium-doped Yttrium Aluminum Garnet
PBL	Planetary boundary layer
Polly	Portable lidar system
RMS	Root mean square
RODOS	Realtime Online Decision Support System for Nuclear Emergency Management in Europe
RL	Residual layer
TKE	Turbulence kinetic energy
UTC	Universal time coordinated
WiLi	Wind lidar
WCT	Wavelet covariance transform

References

Angevine, W., A. Grimsdell, L. M. Hartten, and A. C. Delany (1998). The Flatland Boundary Layer Experiments. *Bulletin of the American Meteorological Society 79*, 419–431.

Bösenberg, J. (2002). Earlinet: A European Aerosol Research Lidar Network to establish an aerosol climatology. Scientific report for the period February 2001 to January 2002. April 2, 2002. Technical report.

Bösenberg, J. and H. Linné (2002). Laser remote sensing of the planetary boundary layer. *Meteorologische Zeitschrift 11*, 233–240.

Brooks, I. M. (2003). Finding boundary layer top: Application of a wavelet covariance transform to lidar backscatter profiles. *Journal of Atmospheric and Oceanic Technology 20*, 1092–1105.

Cohn, S. A. and W. M. Angevine (2000). Boundary layer height and entrainment zone thickness measured by lidars and wind-profiling radars. *Journal of Applied Meteorology 39*, 1233–1247.

Davis, K., N. Gamage, C. Hagelberg, C. Kiemle, D. Lenschow, and P. Sullivan (2000). An objective method for deriving atmospheric structures from airborne lidar observations. *Journal of Atmospheric and Oceanic Technology 17*, 1455–1468.

Engelmann, R. (2003). Entwicklung eines Mini-Ramanlidar und Aufbau einer kombinierten Sende- und Empfangseinheit für ein Doppler-Wind-Lidar. Master's thesis, University of Leipzig.

Engelmann, R., U. Wandinger, A. Ansmann, D. Müller, E. Žeromskis, D. Althausen, and B. Wehner (2007). Lidar observations of the vertical aerosol flux in the planetary boundary layer. *Journal of Atmospheric and Oceanic Technology*, accepted.

Eresmaa, N., A. Karppinnen, S. Joffre, J. Räsänen, and H. Talvitie (2005). Mixing height determination by ceilometer. *Atmospheric Chemistry and Physics 5*,

12698–12722.

Fay, B. (1998). Evaluation and intercomparison of mixing heights derived from a Richardson number scheme and other MH formulae using operational NWP models at the German Weather Service. In *5th International Conference on Harmonisation within Atmospheric Dispersion Modelling, Rhodes, 18-21 May 1998*.

Fay, B. (2005). Operational mixing height scheme at the German Weather Service (DWD). Personal communication.

Fay, B., R. Schrodin, I. Jacobsen, and D. Engelbart (1997). Validation of mixing heights derived from the operational NWP models at the German Weather Service. In S. Gryning, F. Beyrich, and E. Batchvarova (Eds.), *The Determination of the Mixing Height - Current Progress and Problems, EURASAP Workshop Proceedings, 1-3 October 1997,Risø National Laboratory*, pp. 55–58.

Gamage, N. and C. Hagelberg (1993). Detection and analysis of microfronts and associated coherent events using localized transforms. *Journal of the Atmospheric Sciences 50*, 750–756.

Garratt, J. (1992). *The Atmospheric Boundary Layer*. Cambridge University Press, Cambridge/New York/Melbourne.

Hooper, W. P. and E. W. Eloranta (1985). Lidar measurements of wind in the planetary boundary layer: The method, accuracy, and results from joint measurements with radiosonde and kytoon. *Journal of Climate and Applied Meteorology 25*, 990–1001.

Lammert, A. and J. Bösenberg (2005). Determination of the convective boundary-layer height with laser remote sensing. *Boundary-Layer Meteorology 119*, 157–170.

Liljequist, G. H. and K. Cehak (1979). *Allgemeine Meteorologie*. Vieweg & Sohn, Braunschweig/Wiesbaden.

Mattis, I., A. Ansmann, D. Müller, U. Wandinger, and D. Althausen (2004). Multiyear aerosol observations with dual-wavelength Raman lidar in the framework of EARLINET. *Journal of Geophysical Research 109*, 1–15.

Menut, L., C. Flamant, J. Pelon, and P. H. Flamant (1999). Urban boundary-layer height determination from lidar measurements over the Paris area. *Applied Optics 38*, 945–954.

Oke, T. R. (1987). *Boundary Layer Climates*. Routledge, London/New York.

Rhone, P. (2004). Development of the data acquisition and analysis systems for a portable Raman lidar and a Doppler wind lidar. Master's thesis, University of Leipzig.

Russel, P. B. and E. E. Uthe (1978). Regional patterns of mixing depth and stability: Sodar network measurements for input to air quality models. *Bulletin of the American Meteorological Society 54*, 1275–1287.

Steyn, D., M. Baldi, and R. M. Hoff (1999). The detection of mixed layer depth and entrainment zone thickness from lidar backscatter profiles. *Journal of Atmospheric and Oceanic Technology 16*, 953–959.

Stull, R. B. (1988). *An Introduction to Boundary Layer Meteorology*. Kluwer Academic Publishers, Dordrecht/Boston/London.

Weitkamp, C. (Ed.) (2005). *Lidar Range-Resolved Optical Remote Sensing of the Atmosphere*. Springer, New York.

Acknowledgment

This diploma thesis was written from 1 May 2006 to 30 April 2007 at the Leibniz Institute for Tropospheric Research, Leipzig. Therefore, I would like to say thank you to a number of people.
Dietrich Althausen for providing and supervising this diploma work, for proof-reading of the thesis, and for giving me a lot of useful hints. He introduced me into lidar and showed me how to work with Polly.
Albert Ansmann for the continuous support in scientific questions, and the great assistance, especially in the last period of my diploma work.
Ulla Wandinger for the accurate and patient proof-reading, and for the many suggestions how to improve this thesis.
Ronny Engelmann for providing me with information and data of WiLi, and for supplying me with several Labview and IDL tools.
Prof. J. Heintzenberg and Prof. G. Tetzlaff for reviewing this diploma thesis.
The complete "Polly team", which made automated, continuous measurements possible.
Patric Seifert and Matthias Tesche for introducing me in the secrets of LaTeX and IDL, and for adjusting the overlap in clear nights.
The German Meteorological Service (DWD) for providing the LM mixing heights.
Ronny Petrik, Janek Zimmer, Olaf Helmuth and especially Barbara Fay (DWD) for providing me with information about the LM, and answering all the questions about it.
My flat mate Christine Weigelt for doing most of the housekeeping in the last period of this work (and probably even before) and providing me with the necessary distractions.
Last but not least a few words in German to my family: Ein großes Dankeschön gilt meinen Eltern und Großeltern für die geleistete Unterschtützung, sowohl in finanzieller, moralischer oder verpflegungstechnischer Hinsicht. Ihr habt mich bei all meinen Vorhaben immer unterstützt und damit zu einem großen Teil dazu beigetragen, dass diese Arbeit so entstehen konnte.

Statement of authorship

I hereby certify that this diploma/master thesis has been composed by myself, and describes my own work, unless otherwise acknowledged in the text. All references and verbatim extracts have been quoted, and all sources of information have been specifically acknowledged. It has not been accepted in any previous application for a degree.

Leipzig, May 9, 2007

.....
Holger Baars

After positive appraisal of this thesis, I agree that one copy of my presented thesis may remain at the disposal of the library of Leipzig University.

Leipzig, May 9, 2007

.....
Holger Baars